Doctoral Dissertation (Shinshu University)

Study on functional organogelators with electrochemical applications

March 2018

Zhong Wang

Table of contents

List of Figure

List of Table

Chapter 1
Introduction

1.1 Gel

The word “gel” was first used by Thomas Graham, who clipped it from gelatin in 1861. He tried to describe gels ad follow: “while the rigidity of the crystalline structure shuts out external expressions, the softness of the gelatinous colloid partakes of fluidity, and enables the colloid to become a medium for liquid diffusion, like water itself” [1]. Flory then defined a gel, as having a continuous structure that exhibits solid-like rheological behavior and has macroscopic dimensions that are permanent on the time scale of an analytical experiment [2]. Gels were viewed as substantially diluted cross-linked systems that exhibit no flow while in the steady state [3].

1.1.1 Physical and chemical gels

Gels are roughly divided into two types, chemical and physical gels. Chemical gels, which usually have a three-dimensional network structure with covalent bonds formed by polymerization involving multifunctional monomers, are characterized by thermal-irreversibility. Physical gels are usually characterized by dynamic cross-links that are constantly created and broken, causing the gels to change state between solid

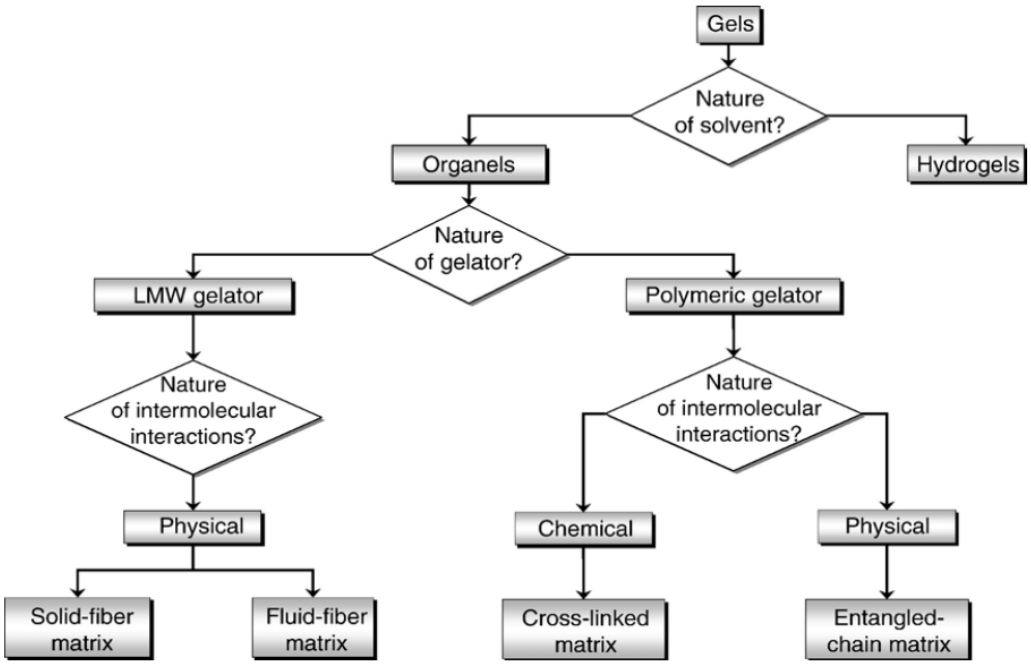

Figure 1.1 Classification of gels

and liquid under the influence of environmental factors [4]. The thermal-irreversibility is due to the robust covalent bonds within the three-dimensional networks. On the other hand, physical gels always reveal thermally-reversible phase transitions between gel and sol, because their networks are formed through weak non-covalent bonds that are easily broken by heating. Among the physical gels, lamellar microcrystals, glassy cross-links, and double helix structures usually lead to strong gels, while H-bonds, block copolymer micelles and ionic associations result in the weak ones.

1.1.2 Organogels and hydrogels

Gels can also be separated into hydrogels and organogels according to the different types of solvent and interaction forces. (Figure 1.1)

The first appearance of a hydrogel was in 1894 [5]. Hydrogels are usually prepared from natural or synthetic hydrophilic polymers which form a colloidal network of polymer chains with water as the dispersion medium. Hydrogels usually performance the similar flexibility compared with natural tissue due to their significant water content. Moreover, hydrogels have many uses such as essential controlled drug delivery [6], cell culture [7] and dressings for wound healing [8].

The demand for organogel based products is increasing because of their easy of preparation and inherent long-term stability [9]. Lately, research on organogels with their applications in food, pharmaceuticals and cosmetics has gained tremendous momentum. Organogels are composed of a liquid organic phase held within a three-dimensional cross-linked network through hydrogen bonding, van der Waals, π–π stacking, and electrostatic interactions. At a critical concentration (the minimum gelation concentration), the network becomes large enough to exhibit the properties of a physical gel, with an extensive continuous solid network, no steady-state flow, and solid-like rheological properties [10]. Organogels exhibit thermal-irreversibility and can accommodate either hydrophilic or hydrophobic compounds within their structure. This property has widened the potential application of organogels, as having their optical and viscoelastic properties, biocompatibility and the potential to be used as drug delivery

agents [11]. Due to their easy spreadability, organogels are becoming a vehicle of choice in different fields. For example, Liu *et al.* reported a shape memory organohydrogel with a heterophase structure, which exhibits an excellent thermomechanical performance and shape memory effect [12]. Yao *et al.* synthesized a self-healable organogel nanocomposite though the condensation of an amino terminated poly(dimethylsiloxane) (NH_2-PDMS-NH_2) and isophorone diisocyanate (IPDI), with angle-independent structural colors and surface slipperiness, which could be useful in color-related areas [13]. In general, organogels gained countless applications in many areas, including cosmetics and food. The scope of organogels is expected to increase further, since their manufacture is easy and cost effective. Generally, gels, especially physical gels, are unstable systems because of the balance between molecular aggregation forces and solubilizing gelator-solvent interactions, and gelation is a spontaneous, thermodynamically and kinetically driven process [14].

1.1.3 Polymer gels and low-molecular-weight gelators

Gels can also be divided into polymer gels and low-molecular-weight gelators (LMWGs).

Polymer gels immobilize solvent molecules by forming a network of either cross-linked or entangled chains for chemical and physical gels. And they can be classified into three categories: those that form supramolecular crosslinking points through conformational changes, those formed by addition of crosslinking agents, and those formed by self-assembly of gelation-causing segments [15]. Many polymer organogelators have been reported, including polypeptides [16], poly(ethylene glycol) [17], poly(propylene glycol) [17] and other.

LMWGs which can form supramolecular gels have captured significant interest with their unique properties and wide potential applications as soft materials in several fields [18]. LMWGs are usually driven by non-covalent intermolecular forces such as hydrogen bonding, van der Waals forces, π–π stacking, and electrostatic interactions [19]. Non-covalent crosslinks and physical entanglements within the supramolecular

structure build a three-dimensional network, and solvent is immobilized into the nanostructure.(Figure 1.2) In most cases, gelation by LMWGs produces gels with remarkably low mechanical strength compared with polymer gels. LMWGs constitute an ocean of nanostructures, such as nanofibers, nanoribbons, nanoparticles, helices, nanosheets and bundle structures. LMWGs are thus characterized by their ability to form several types of nanostructure in suitable solvents [20]. With these advantages, LMWGs have been widely researched. For example, Shinkai *et al.* reported π-block-based low-molecular-weight gelators based on tetrathiafulvalene (TTF) core that gave extremely elongate π-stacked assemblies though strong π-π interactions, and indicated that LMWGs could be used for novel soft materials for electrochemistry [21]. Garcia-Frutos *et al.* focused on researching organic light-emitting devices (OLEDs) formed from organogels due to their outstanding suitability for optoelectronics applications. They reported self-assembling organogels, 5-(4-nonylphenyl)--7-azaindoles, which exhibited an excellent performance as a part of OLEDs [22].

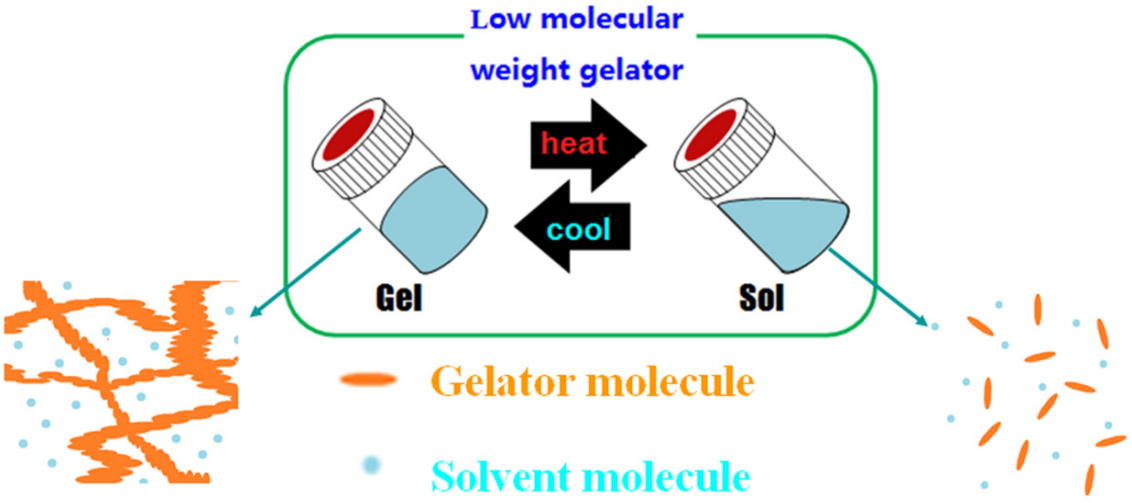

Figure 1.2 Gel-sol transition of LMWGs.

1.2 Batteries

1.2.1 History

The use of the word batteries to describe a group of electronic devices is credited by Benjamin Franklin. Italian physicist Alessandro Volta manufactured and described the first electrochemical battery called the voltaic pile in 1800 (Figure 1.3). That was a stack of copper and zinc plates, separated by brine-soaked paper disks, and it produced a steady current for a considerable length of time. Although, in early stage, batteries were of great value for experimental purposes, their voltages fluctuated and they could not provide a large current for sustained period of time. The Daniell cell was the first practical source of electricity and saw widespread adoption as a power source for electrical telegraph networks [23]. It consisted of a copper pot filled with a copper sulfate solution, in which was immersed an unglazed earthenware container filled with sulfuric acid and a zinc electrode. A battery consists of two half-cells connected in series with a conductive electrolyte containing anions and cations. One half-cell includes electrolyte and a negative electrode, while the other contains electrolyte and a positive electrode.

In 1839, William Robert Grove from England successfully synthesized the first fuel cell. Georges-Lionel Leclanche synthesized the dry Leclanche cell with NH_4Cl electrolyte and commercialized it in 1888. Another scientist named Gaston Planté developed a lead-acid battery based on the Leclanche's work. In 1899, the nickel-cadmium battery was manufactured. After World War Two, the battery developed

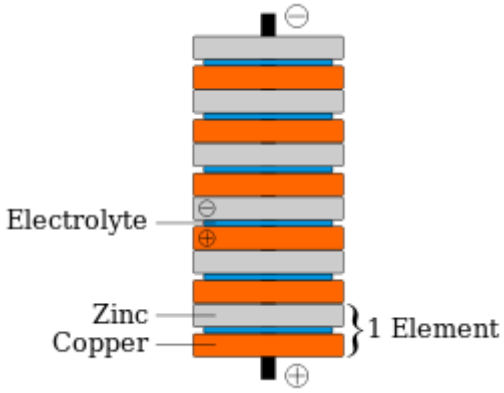

Figure 1.3 Configuration of Voltaic pile.

rapidly with breakthroughs in basic theory, novel electrode materials and new equipments. These led to the silver-zinc battery, the alkaline manganese-zinc battery, the Ni-metal hydride battery, and the lithium battery. The Sodium-sulfur battery was also produced . The most attractive one was the lithium battery.

Li metal has the smallest density (0.534g cm^{-1}, 20 ℃) and the lowest standard electrode potential (-3.045 V vs. SHE) with the theoretical capacity of 3,860 mAh g^{-1}. The first commercialized lithium battery was used as cardiac pacemaker with a lithium-iodine battery [24]. Its energy density was five times that of a traditional Zn-HgO battery and it had a service life of 6-7 years. Scientists thus focused on the lithium-ion battery, which had the potential applications as a secondary battery. Owing to their competitive energy and power density, lithium-ion batteries (LIBs) have conquered the rechargeable battery market and have numerous potential applications in electronic devices. Since the 1970s, when LIBs were invented, they have been used worldwide and a lot of research has been dedicated to further improving their performance including energy density, power density, and cycle life [25]. LIBs, as chargeable secondary batteries, could be manufactured in several different shapes, such

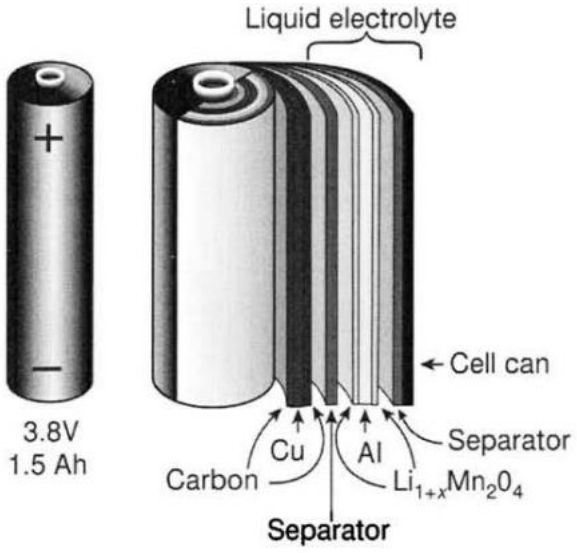

Figure 1.4 Inner structure of columnar batteries

as button batteries, columnar batteries, and square batteries. Usually, LIBs consist of a cell casing, a current collector (aluminum foil and copper foil), cathode materials, an electrolyte, a seperator, and anode materials, as shown in Figure 1.4. Figure 1.5 shows the working principle of a lithium-ion battery.

1.2.2 Anodes

The anode materials are an important part of LIBs, and they have a significant influence on the battery performance. The ideal anode materials should have the following characteristics:

(1) They should allow more lithium ions to be reversibly insertion and deinsertion, in order to increase their capacity and thus increase charge storage.

(2) They should have a low voltage platform, to provide a higher working voltage.

(3) During the insertion process with the lithium ions, the anode materials should be sufficiently stable.

(4) Excellent ionic and electronic conductivity would reduce the electrochemical polarization.

(5) They should exhibit chemical stability at the operating voltage

Currently, research on anode materials focuses on the following three types: carbon materials like graphite and graphene; alloy materials like Si and Sn; and metal oxides or metal sulfides like Fe_2O_3, CoO and CoS_2 [27].

Since the commercialization of LIBs, graphite has been the most widely used anode material. Its most attractive property is the low potential in lithium intercalation (~0.1 V). Its other advantages are high specific mass capacity and specific volumetric capacity, easy of forming stable SEI films, absence of side reactions with liquid electrolytes, and high ionic conductivity. However, graphite is easily separated during charge and discharge process with lithium ions and solvent ions, which reduces the stability of the battery. Also, with a rapid charge and discharge process, it is difficult to intercalate all the lithium ions into the graphite layer; thus, some lithium ions would

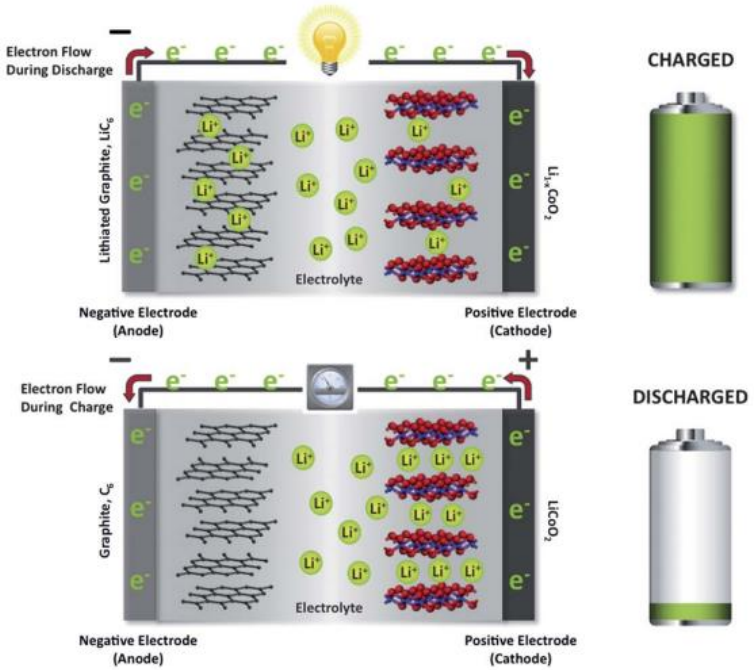

Figure 1.5 A schematic illustration of the working Principle of lithium ion battery [26].

aggregate on would aggregate on the surface of the graphite, resulting in a the low capacity and even security risks [28]. Besides graphite, amorphous carbon [29], carbon nanotubes [30] and graphene [31] have also been researched.

The principle of alloy materials is different for graphite. Lithium was reacted with the anode materials to form an alloy. For example, with Sn as the anode, the equation can be represented as follows:

$$Sn + xLi^+ + xe^- \underset{\text{Charge}}{\overset{\text{Discharge}}{\rightleftharpoons}} Li_xSn \ (X<4.4)$$

These types of alloy usually have an extremely high theoretical capacity. For example, the theoretical capacity of Sb metal is 660 mAh g^{-1} [32], while that of Sn is 992 mAh g^{-1} [33]. They also have a higher capacity than graphite. However, these types of material have a huge drawback. With the alloying process, the volume of the anode would change considerably, even by more than 200%. This would affect the cycling performance and create security risks. With further research, to reduce the size of the

materials, porous structures [34] and composites [35] had been carried out to overcome these problems.

The last part of anode materials to be developed was metal oxides and sulfides. They usually reacted with lithium ions to form lithium oxides and elemental metal.

$$MO_x + 2xLi^+ + 2xe^- \underset{\text{Charge}}{\overset{\text{Discharge}}{\rightleftharpoons}} M + xLi_2O$$

The reaction principle is shown in Figure 1.6. Owing to the special reaction principle, the theoretical capacity is generally over 600 mAh g^{-1}. They also have some drawbacks include low ionic conductivity, volume inflation and decomposition of the liquid electrolytes.

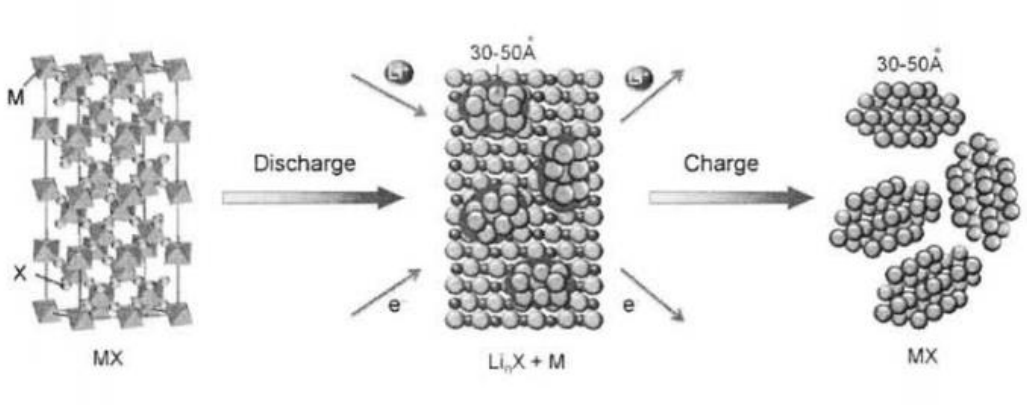

Figure 1.6 Reaction principle of metal oxides

1.2.3 Cathodes

Table 1.1 Comparison of the properties of traditional cathodes [38].

Property	$LiAl_{0.05}Co_{0.15}Ni_{0.8}O_2$	$LiCoO_2$	$LiMn_2O_4$	$LiFePO_4$
Avg. voltage(V)	3.65	3.84	3.86	3.22
Theo. Capacity(mAh g^{-1})	265	274	117	170
Density(g cm^{-3})	4.73	5.05	4.15	3.60
Specific energy(Wh kg^{-1})	219.8	193.3	154.3	162.9
Energy density(Wh L^{-1})	598.9	557.8	418.6	415.0

Cathode materials for the lithium-ion battery were first reported in 1980, where $LiCoO_2$ was used as a cathode material [36]. Since the C/ $LiCoO_2$ commercial battery was introduced by Sony, LIBs have been widely used in electronic storage devices. As an important part of the battery, the cathode materials determine its energy density and operating voltage of the battery. Traditionally, there are three types of cathode materials; hexagonal layered structures as $LiCoO_2$, spinel type structures as $LiNi_{0.5}Mn_{1.5}O_4$ and $LiMn_2O_4$ and olivine type structures as $LiFePO_4$ [37]. Some novel cathode materials were also researched, as organic polymers had attracted the attention of scientists and these will be discussed later.

$LiCoO_2$ was the first commercialized cathode material, which had the advantages of high capacity, high operating voltage, stable charge/discharge curves and excellent coulomb efficiency. $LiCoO_2$ showed a layer structure where lithium ion diffusion between the layers. During charging, Li^+ ions are deinserted from the CoO_2 layers with a theoretical capacity of 274 mAh g^{-1}. In fact, only about 50% of the lithium ions can be deinserted. This phenomenon is caused by structure changes accompanying the lithium deinsertion. Promotion of deintercalation would result in the precipitation of oxygen, decomposition of the electrolyte and dissolution of the CoO_2. As common, the top cut-off voltage for the batteries was 4.2 V with $LiCoO_2$. In this case, the true capacity is about 137 mAh g^{-1}. Otherwise, Co metal is toxicity, which is dangerous when leakage occurs. To solve these problems, Al, Mn and Ni are carried out to replace the Co. Ohzuku *et al.* reported a novel lithium insertion materials $LiCo_{1/3}Ni_{1/3}Mn_{1/3}O_2$ which has 200 mAh g^{-1} of rechargeable capacity between the voltages of 2.5 V and 4.6 V [39].

The reaction principle of $LiMn_2O_4$ cathode materials is the same as that of $LiCoO_2$. In addition, to being a cheap and non-toxic alternative material, the spinel structure of $LiMn_2O_4$ provides a three-dimensional framework for the insertion and deinsertion of Li^+ ions during discharge and charge of the battery. A novel kind of spinel structure cathode was $LiNi_{0.5}Mn_{1.5}O_4$. Compared with $LiCoO_2$, its operating voltage has been increased to 4.7 V, which presents the high energy density [40]. There are two types of

$LiNi_{0.5}Mn_{1.5}O_4$ depending on the ordering of Ni/Mn in the octahedral sites, disordered and ordered. In the disordered spinel, transition-metal ions are randomly distributed at octahedral 16*d* sites, presenting the *Fd*3*m* space group (Figure 1.7(a)). In contrast, the ordered $LiMn_2O_4$ has a $P4_332$ space group (Figure 1.7(b)) [41].

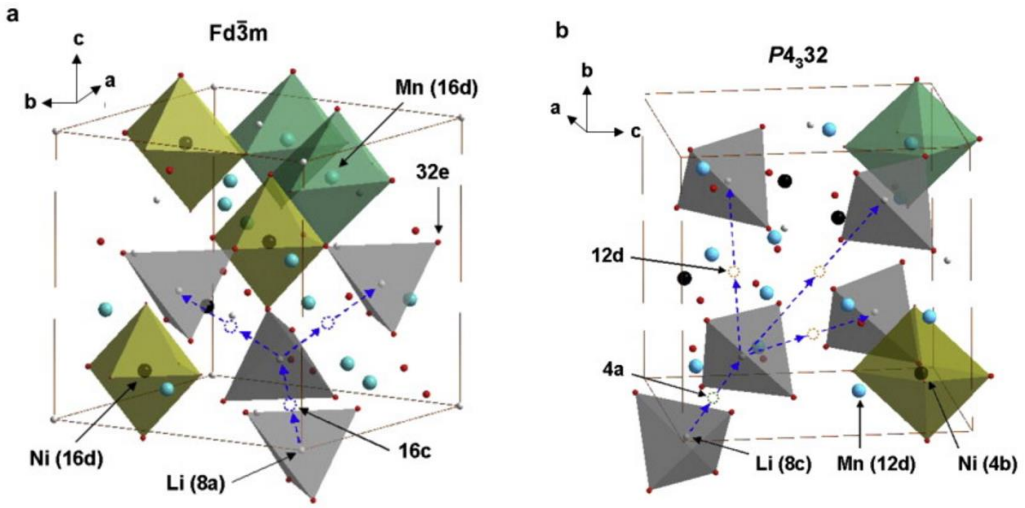

Figure 1.7 Lithium diffusion path in $LiMn_{1.5}Ni_{0.5}O_4$ spinel with space group of (a) *Fd*3*m* and (b) $P4_332$ [41]

The application of $LiFePO_4$ was first proposed by Goodenough [42,43]. The insertion voltage of the lithium ion in $LiFePO_4$ was about 3.5 V, with a theoretical capacity of 170 mAh g^{-1}. Although the energy density was not good enough compared with others, the stability of olivine structure during the deinsertion process make it attractive. The greatest improvement in the performance is the electronic conductivity (1×10^{-9} S cm^{-1}, rt.) and ion conductivity ($1.8\times10^{-14}cm^2$ s^{-1}, rt.).

1.2.4 Electrolytes

Electrolytes are ubiquitous and indispensable in all electrochemical devices, and their basic function is independent of the much diversified chemistries and applications of these devices. The electrolyte of a battery usually consists of soluble salts, acids or

other bases in liquid, gelled and dry formats. When electrodes are placed in an electrolyte and a voltage is applied, the electrolyte will conduct electricity. Lone electrons cannot normally pass through the electrolyte; instead, a chemical reaction occurs at the cathode, providing electrons to the electrolyte. Another reaction occurs at the anode, consuming electrons from the electrolyte. As a result, a negative charge cloud develops in the electrolyte around the cathode, and a positive charge cloud develops around the anode. The ions in the electrolyte neutralize these charges, enabling the electrons to keep flowing and the reactions to continue. Because of its physical location in electrochemical devices, the electrolyte interacts closely with both of the anode and cathode. The interfaces between the electrolyte and anode/cathode always dictate the performance of the devices. Figure 1.8 shows the classification of the electrolytes.

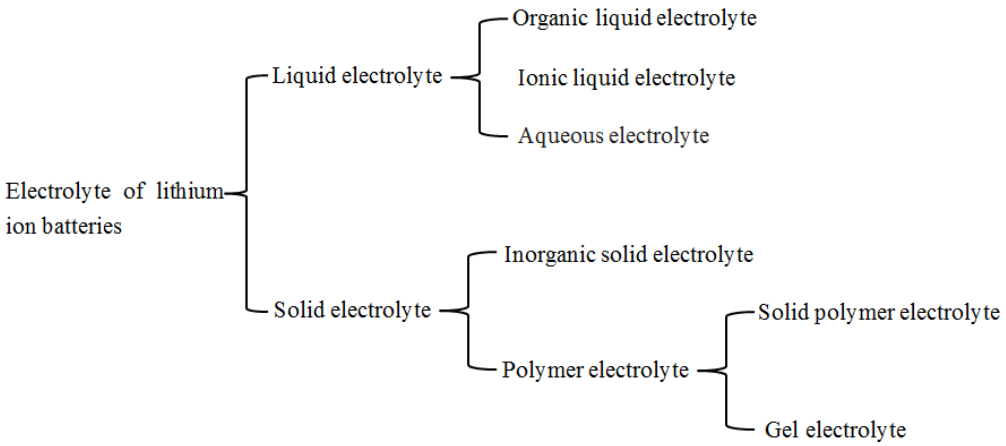

Figure 1. 8 The classification of electrolyte in LIBs.

A traditional lithium ion battery use a polar solvent and lithium ions as the electrolyte, which usually has the advantages of high conductivity, low cost, high ionic transformation speed, and long cycle life. The following tables show some physical parameters of the organic solvents and lithium salts. (Table 1.2 and Table 1.3) Most compositions of lithium electrolytes are based on solutions of one or more lithium salts in mixtures of two or more solvents. The rationale behind the mixed solvent formulation

is that the diverse and contradicting requirements of battery applications can hardly be met by any individual compound, as high fluidity versus high dielectric constant. Therefore, solvents with very different physical and chemical properties are combined together to perform the various functions simultaneously [44]

Table 1.2 The physical parameters of some organic solvents in LIBs. (25 ℃) [44]

solvent	Melting point (℃)	Boiling point (℃)	Relative permittivity	Viscosity (cP)
EC	36.4	248	89.78	1.90 (40 ℃)
PC	-48.8	242	64.92	2.53
DEC	-43	126	2.805	0.75
DMC	4.6	91	3.107	0.59
EMC	-53	110	2.958	0.65
γ-BL	-43.5	204	39	1.73

Table 1.3 The physical parameters of some lithium salt. [44]

Name	formula	Molecular weight	Melting point (℃)	σ (mS cm^{-1}) (25 ℃)	
				PC	EC:DEC= 1:1, (v/v)
Lithium perchlorate	$LiClO_4$	106.4	236	5.6	8.4
Lithium tetrafluorobo--rate	$LiBF_4$	93.9	293	4.59	4.9
Lithium hexafluoroar--senate	$LiAsF_6$	195.9	340	5.7	11.1
Lithium hexafluoro--phosphate	$LiPF_6$	151.9	200	5.8	10.7
LiTFSI	$Li[N(SO_2CF_3)_2]$	287.1	234	5.1	9.0

An ideal electrolyte solvent should meet the following requirements. (1) It should be able to dissolve suitable salts to sufficient concentration. In other words, it should have a high dielectric constant (σ). (2) It should have low viscosity to fit for the facile ion transport. (3) It should remain inert to all cell components, especially the charged surfaces of the cathode and the anode, during cell operation. (4) It should remain liquid within the operating temperature range, i.e. have a low melting point and high boiling point. (5) It should be low toxicity. For LIBs, the lithium salts must be soluble in non-aqueous compounds. Since the inception of non-aqueous electrolytes, a wide spectrum of polar solvents has been investigated, and the majority of them fall into either one of the following families: organic esters or ethers [44]. All the ethers, including cyclic and acyclic, demonstrate similar dielectric constants and low viscosities, while for the ester, it looks like different kinds of compound with cyclic and acyclic structure. Among these solvents, cyclic esters of carbonic acids have attracted most of the research attention, especially during the past decade, when their role in forming an SEI on carbonaceous anodes became recognized.

Lithium salts were also an important part of the electrolyte. An ideal electrolyte salt for LIBs should meet the following requirements. (1) It should be able to dissolve and dissociate in non-aqueous media. (2) It should be stable with respect to oxidative decomposition at the cathode. (3) It should be inert in the electrolyte solvent. Dahn *et al.* described over 150 electrolyte solvent compositions based on 27 basic solvents but only 5 types of lithium salt [45]. This is because the ionic radius of the lithium ion is too small, which caused the lithium simple salts could not satisfy the minimum solubility requirement in low dielectric media. Soft Lewis bases such as Br^- and I^-, are oxidized on the charged surfaces of the cathode below 4.0 V vs. Li. Most of the lithium salts that are qualified for the minimal solubility standard are based on complex anions that are composed of a simple anion core stabilized by a Lewis acid agent. The requirement for chemical inertness further excludes a family of lithium salts as $LiAlX_4$, which was widely used in lithium batteries [46]. The $AlX4^-$ ions also cause the corrosion of other

components in cells, as separators (usually PP) and insulating sealants. On the other hand, anions that based on milder Lewis acids, as ClO_4^-, BF_6^-, PF_6^- and AsF_6^-, have exhibited stablility with organic solvents. The average ion mobility and the dissociation constant of the lithium salt with milder Lewis acids were shown as follows:

Average ion mobility: $LiBF_4 > LiClO_4 > LiPF_6 > LiAsF_6$

Dissociation constant: $LiAsF_6 > LiPF_6 > LiClO_4 > LiBF_4$

According to ionic studies on the limiting properties of various solvents, this excellent conductivity results from the combination of its ionic mobility and dissociation constant, although in neither category does $LiPF_6$ stand at the most outstanding position.

Nowadays, in most cases, $LiPF_6$ is used as the solute, EC as the solvent, and DEC, DMC or EMC as cosolvents.

Since aqueous rechargeable lithium batteries (ARLBs) using positive electrode materials from commercial LIBs were first introduced in 1994, they have attracted wide attention as promising systems because of their low capital investment, environmental friendliness and good safety [47]. They are a suitable alternative because their energy density can be above that of the corresponding LIBs. They usually use Li_2SO_4 and $LiNO_3$ as the solute, while using LiOH to adjust the pH of the electrolyte. The advantages of the aqueous system were: (1) high ionic conductivity due to the high dielectric constant and low viscosity; (2) low cost; and (3) easy of manufacture. Although an aqueous electrolyte would be safer and more environmentally benign, the electrochemical window is 1.23 V, which precludes the use of high voltage electrode couples with high energy density of LIBs. Wu *et al.* reported an aqueous lithium ion battery using graphite coated with gel polymer electrolyte (GPE) and Lithium super ionic conductor (LISICON) as the negative electrode, $LiFePO_4$ in 0.5 mol L^{-1} Li_2SO_4 aqueous solution as the positive electrode, performance discharge voltage of 3.1 V and an energy density of 258 Wh Kg^{-1} [47].

An ionic liquid solvent usually consists of organic cations and inorganic/organic

anions. Ionic liquids possess high ionic conductivity and broad electrochemical windows. In general, there are several types of ionic solvents: tetraalkylammonium, phosphonium, sulfonium, pyrrolidium, piperidinium, morpholinium, imidazolium, pyridinium, pyrazolium, pyrrolinium and guanidinium. Of these solvents, the most popular are immidazolium and tetraalkylammonium types. The advantages of ionic liquids were: (1) stable electrochemical windows over 5 V; (2) high ionic conductivity, even up to 10^{-2} S cm^{-1}; (3) non-volatility; and (4) high boiling point. Therefore, the ionic liquid could function as an electrolyte in energy storage devices. Indeed, traditional LIB electrolytes are mixtures of organic solvents like EC, DMC, DEC and PC mainly with $LiPF_6$ as the solute. These still require further research compared with organic or aqueous liquid electrolytes.

Solid electrolytes, which are electrically conductive solids with ionic carriers, have received special attention because of their potential use in solid state batteries, fuel cells, energy storage, and chemical sensors [48]. The development of the solid electrolyte is shown in Figure 1.9. The history of solid-state ionic conductors dates back to the 1830s, when Faraday discovered the remarkable property of conduction in heated solids Ag_2S and PbF_2 [50].

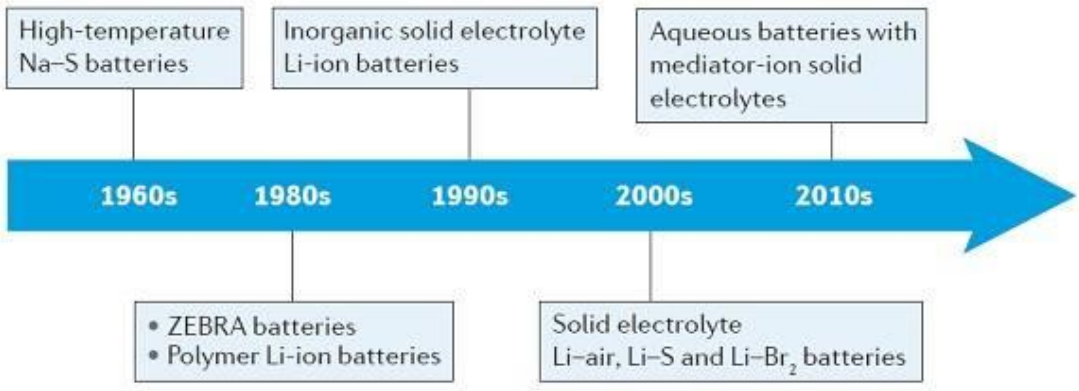

Figure 1.9 The development of the solid battery. [49]

Inorganic solid electrolyte was first reported by E. Warburg as a type of ion conductor in 19 century. It had the advantages of high ionic conductivity (>10^{-3} S cm^{-1}), low activation energy and high energy density. It could be separated into two types according to physical structure: crystalline solid and glassy solid materials. In the crystalline material, the representative materials are perovskite, NASICON (Na super ionic conductor), LISICON, LiPON. Oxide/sulfide materials are on behalf of the glassy type. They can also be divided into one-dimensional, two-dimensional (as Al_2O_3, Li_3N), three-dimensional ion conductors (as LISICON, NASICON) according to the conductivity. An inorganic solid electrolyte should meet the following requirements [51]; (1) excellent ionic conductivity at operating temperature; (2) low electronic conductivity; (3) chemical stability; and (4) high chemical decomposition voltage (> 5.5 V vs. Li^+/Li).

Solid polymer electrolytes (SPE) which are solvent-free electrolytes based on polymers have potential for use in next-generation LIBs. It was first reported by Wright in 1973, who described a PEO-alkali metal salt complex with ionic conductive behaviour. As a replacement of liquid electrolyte, it has several advantages: (1) it allows the use of higher energy density solid lithium at the anode; (2) it removes toxic solvents; (3) it improves the cycling ability; and (4) it eliminates the need for heavy casings. Despite the advantages of SPE, their ionic conductivity is insufficient for use in batteries. Therefore, two measurements have been carried out to increase the ionic conductivity of the SPE: (1) the suppression of crystallization of polymer chains to improve polymer chain mobility; and (2) increase in the carrier concentration. The suppression of crystallization of polymer chains can be realized by (1) cross-linking; (2) copolymerization; (3) comb formation (side chains and dendritic polymers); (4) a polymer alloy (including Inter Penetrating Network (IPN)), and (5) inorganic filler blensd. Among these, combinations of (1) cross-linking; (2) copolymerization, and (3) comb formation are useful for obtaining a high ionic conductivity [52]. Of the SPEs, PEO as a type of lithium salt storage component has been widely researched. The oxygen atom in the PEO has lone pairs, while the Li^+ has the unoccupied 2s orbital, thus,

they can form a coordination structure on the PEO chains, and through the coordination and dissociation process, to induce movement of the Li^+ in the PEO polymer.

A GPE is a type of electrolyte that is neither liquid nor solid, and has the advantages of both liquid and solid electrolytes. Gels possess both the cohesive properties of solids and diffusive properties of liquids. A GPE is a hybrid system formed by trapping a large amount of liquid electrolyte a lithium-ion conducting organic solvent in a polymer matrix (e.g. PEO, PMMA and PVC) [53].The GPE was developed according to the following two concepts: (1) physical cross-linking; and (2) chemical cross-linking. (Figure 1. 10)

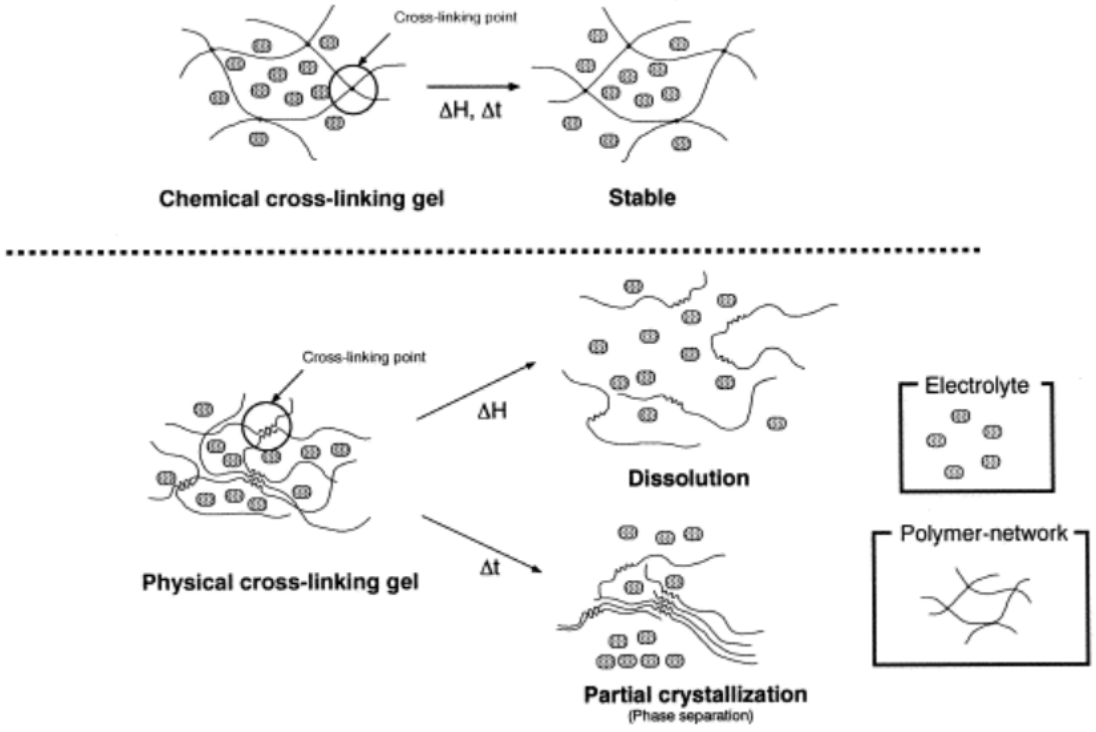

Figure 1.10 Chemical and physical GPE structures. [52]

For a GPE, the transfer of lithium-ions mainly depends on the swollen gelled phase or the absorbed liquid electrolyte. A GPE system has high ionic conductivity, good mechanical strength, better flexibility, wide electrochemical window, good

compatibility with electrodes, and an improved capability for trapping liquid electrolytes compared to conventional separators. In addition, the excellent thermal stability of GPEs could lead to the improvement of safety for the LIBs, and the encapsulated liquid electrolyte in a solid polymer host can lead to enhanced electrode/electrolyte interface stability toward both electrodes [53]. Many gel polymers such as poly(ethylene oxide) [54], poly(vinylidene fluoride) [55], poly(methyl methacrylate) [56], and polyacrylonitrile [57] have been widely reported.

As well as these GPEs, some LMWGs have been used to convert liquid electrolytes for LIBs to gel via the formation of 3D fibrous networks through intermolecular interactions such as hydrogen bonding and van der Waals force. Yanagida *et al.* used 1-hexyl-3-methylimidazolium iodide, iodine, and an L-isoleucine-based LMWG to fabricate quasi-solid-state dye-sensitized solar cells (DSCs) with high stability and good performance [58]. Tritt-Goc and co-workers reported a series of LMWG electrolytes based on methyl-4,6-O-(p-nitrobenzylidene)--α-D-glucopyranoside and a quaternary ammonium salt (TMABr) electrolyte solute, which produces recoverable iongels with potential applications in electrochemical cells [59].

1.3 Radical materials

In chemistry, a radical is an atom, molecule or ion that has an unpaired valence electron. These unpaired electrons make free radicals highly chemically reactive. The first radical was observed by Moses Gomberg in 1900, called triphenylmethyl radical. The formation of radicals may involve the breaking of covalent bonds by homolysis, a process that requires significant amounts of energy. Radical formation through homolytic bond cleavage usually occurs between two atoms of similar electronegativity; in organic chemistry, this is often between the O–O bonds in peroxide species or between O–N bonds. Radicals may also be formed by single-electron oxidation or

reduction of an atom or molecule. Although radical ions exist, most species are electrically neutral.

Generally, radicals are short-lived due to their reactivity, although there are some long-lived radicals: stable radicals, persistent radicals and diradicals. Prime examples of stable radicals are molecular dioxygen (O_2) and nitric oxide (NO). Diradicals are molecules containing two radical centers, and multiple radical centers can exist in one molecule. The most widely researched long-lived radicals are the persistent radicals. These employ steric crowding around the radical center to make it physically difficult for the radical to react with other molecules [60]. For example, the four α-methyl groups of nitroxide in TEMPO work to make the radical groups stable. Examples of these include the triphenylmethyl radical, potassium nitrosodisulfonate, nitroxides and nitronyl nitroxide.

Nitroxides, as stable organic radicals, represent an interesting class of molecules that form the basis of novel and emerging functional materials such as radical batteries [61], spin probes [62], polarizing agents for DNP-NMR [63,64], antioxidants[65], magnetoactive materials [66], and radiation protective agents [67] owing to their single component charge-transfer properties [68]. 2,2,6,6-tetramethyl-piperidine 1-oxyl free radical (TEMPO) is the representative of the nitroxide. It was discovered by Lebedev and Kazarnowskii in 1960 [69] and is prepared by oxidation of 2,2,6,6-tetramethyl--piperidine.

In chemicals reactions, TEMPO usually works as a catalyst for the oxidation of primary alcohols to aldehydes. TEMPO oxidations also exhibit chemical selectivity, being inert toward secondary alcohols, but the reagent will convert aldehydes to carboxylic acids. It can also be employed in nitroxide mediated radical polymerization, a controlled free radical polymerization technique that allows better control over the final molecular weight distribution. The TEMPO free radical can be added to the end of a growing polymer chain, creating a "dormant" chain that stops polymerizing. However, the linkage between the polymer chain and TEMPO is weak, and can be broken by

heating, which then allows the polymerization to continue. Thus, chemists can control the extent of polymerization and synthesize narrowly distributed polymer chains.

Recently, the use of TEMPO as a cathode material has been popular. Radical polymers are aliphatic or non-conjugated polymers with organic robust radicals as pendant groups in each repeating unit. The redox sites in radicals allow efficient gradient-driven electron transport through the polymer layer via outer self-exchange reactions in the presence of an electrolyte. Among radical polymers, poly(2,2,6,6-tetramethylpiperidinyloxy-4-yl methacrylate) (PTMA), a derivative of polymethacrylate with a TEMPO radical in its repeating unit exhibited high capacity, a good rate performance and a long cycle life when used as a cathode material for LIBs. PTMA was originally studied as a cathode material by Hasegawa and co-workers [70] in 2002 and further developments have been proposed by Nishide and Suga [71,72]. Li *et al.* used graphene-grafted PTMA and reduced graphene oxide as cathode materials in a cell that showed a two-electron redox reaction mode, providing a high capacity of 466 mA h g^{-1} [73].

1.4 The purpose of this study

With a growing demand for renewable energy, the demand for green LIBs is continuously increasing. The cathode materials generally used in LIBs are inorganic materials (e.g., $LiCoO_2$, $LiMnO_4$), which have some drawbacks related to their limited theoretical capacity, unrenewable resources, and large energy consumption. Organic compounds, which can be prepared by environmentally benign processes, have been investigated as renewable resources. Organic materials also have the advantage of diversity; different side chains or structures, so they can performance different properties though easy syntheses.

1.5 Contents of this study

In this study, the purpose of the studies was carried out within the following aspects of the work:

(1) Investigation of gel electrolyte.

Cyclo(L-β-3,7-dimethyloctylasparaginyl-L-phenylalanyl) was used as a gelator to synthesize gel electrolytes with 1-butyl-3-methylimidazolium tetrafluoroborate, propylene carbonate, and γ-butyrolactone in 1 M $LiBF_4$. Gel strengths and thermal stabilities were studied with respect to the effect of graphite as an additive. Ionic conductivities, activation energies for ionic conductivity, and the electrochemical stabilities of the graphite-containing gel electrolytes were also studied.

(2) Functional gelators with electrochemical properties.

Low-molecular-weight gelators bearing 2,2,6,6-tetramethylpiperidine-1-oxyl (TEMPO) were synthesized by amidation reactions with DiC and DMAP. The gelators formed thermal-reversible gels in various organic solvents and electrolytes. The minimum gelation concentration against γ-BL containing lithium salts increased as compared to that of neat γ-BL. The increase in the minimum gelation concentration is due to the dielectric constant of γ-BL increasing as a result of addition of lithium salt. TEM images of the loose xerogel in γ-BL exhibited clear fibers with a diameter of ~100 nm, while the image of γ-BL including lithium salts showed slender fibers, suggesting the interruption of fibers growth by lithium salts. The strengths of the gels containing lithium salts decreased as compared to that of neat γ-BL, indicating that the lithium salts obstructed the growth of fibrous aggregation. Electrochemical measurements, including cyclic voltammetry and cell performances confirmed the redox properties and showed a plateau output voltage with a rapid charging-discharging process.

In this study, I prospect to manufacture a type of soft battery with organic cathode and LMWG electrolytes which has the properties of flexible and safe. This type of battery might be used on the clothes with the flexibility. There would also be no problems associated with dangerous high temperatures due to the gel-sol phase transition, which would act as a safety mechanism by preventing the battery from

working.

1.6 References

[1] R. G. Weiss, P. Terech. Molecular Gels: Materials with Self-Assembled Fibrillar Networks, Springer, Netherlands, **2006**.

[2] P. J. Flory, Gels and gelling process. *Faraday Discussions of the Chemical Society*, **1974**, *57*, 7-18.

[3] J. D. Ferry, 'viscoelastic properties of polymers, Wiley-VCH, New York, **1980**.

[4] Y. An, F. J. Solids, H. Jiang, A thermodynamic model of physical gels. *J. Mech. Phys. Solids*, **2010**, *58*, 2083-2099.

[5] J. M. Bemmelen, Der Hydrogel und das kristallinische hydrat des kupferoxydes, *Colloid. Ploym. Sci*. (Zeitschrift für Chemie und Industrie der Kolloide), **1907**, *1*, 213-214.

[6] A. C. Mendes, A. N. Zelikin, Enzyme Prodrug Therapy Engineered into Biomaterials, *Adv. Funct. Mater*., **2014**, *24*, 5202-5210.

[7] J. Thiele, Y. Ma, S. M. C. Bruekers, S. Ma, W. T. S. Huck, Designer Hydrogels for Cell Cultures: A Materials Selection Guide, *Adv. Mater.*, **2014**, *26*, 125-148.

[8] L. Zhang, Y. Ma, X. Pan, S. Chen, H. Zhuang, S. Wang, A composite hydrogel of chitosan/heparin/poly(γ-glutamic acid) loaded with superoxide dismutase for wound healing, *Carbohyd. Polym.*, **2018**, *180*,168-174.

[9] K. Hanabusa, K. Hiratsuka, M. Kimura, H. Shirai, Easy Preparation and Useful Character of Organogel Electrolytes Based on Low Molecular Weight Gelator, *Chem. Mater.*, **1999**, *11*, 649-655.

[10] S. R. Raghavan, J. F. Douglas. The conundrum of gel formation by molecular nanofibers, wormlike micelles, and filamentous proteins, *Soft Matter*, **2012**, *8*, 8539-8546.

[11] X. Punet, R. Levato, I. Bataille, D. Letourneur, E. engel., M. A. mateos-Timoneda,

Polylactic acid organogels as versatile scaffolding technique, *Polym.*,**2017**, *113*, 81-91.

[12] Z. Zhao, K. Zhang, Y. Liu, J. Zhou, M. Liu, Highly Stretchable, Shape Memory Organohydrogels Using Phase-Transition Microinclusions, *Adv. Mater*. **2017**, *29*, n/a

[13] J. Zhou, P. Han, M. Liu, H. Zhou, Y. Zhang, J. Jiang, P. Liu, Y. Wei, Y. Song, X. Yao, Self-healable Organogel Nanocomposite with Angle-Independent Structural Colors, *Angew. Chem. Int. Ed*., **2017**, *56*, 10462-10466.

[14] X. Liu, J. Fei, A. Wang, W. Cui, P. Zhu, J. Li, Transformation of Dipeptide-Based Organogels into Chiral Crystals by Cryogenic Treatment, *Angew. Chem. Int. Ed.*, **2017**, *56*, 2660-2663.

[15] M. Suzuki, K. Hanabusa, Polymer organogelators that make supramolecular organogels through physical cross-linking and self-assembly, *Chem. Soc. Rev.*, **2010**, *39*, 455-463.

[16] R. Tadmor, R. L. Khalfin, Y. Cohen, Reversible Gelation in Isotropic Solutions of Helical Polypeptide Poly(γ-benzyl-L-glutamate): Kinetics and Formation Mechanism of the Fibrillar Network, *Langmuir*. **2002**, *18*, 7146-7150.

[17] M. Suzuki, S. Owa, H. Shirai, K. Hanabusa, New poly(propylene glycol)- and poly(ethylene glycol)- based polymer gelators with L-lysine, *Macromol. Rapid Commun.*, **2005**, *26*, 803-807.

[18] P. Terech, R. G. Weiss, Low-Molecular Mass Gelators of Organic Liquids and the Properties of their Gels, *Chem. Rev.*, **1997**, *97*, 3133-3159.

[19] H. Hoshizawa, Y. Minenura, K. Yoshikawa, M. Suzuki, K. Hanabusa,Thixotropic Hydrogelators Based on a cyclo(dipeptide) Derivative, *Langmuir*, **2013**, *29*, 14666-14673.

[20] M. Suzuki, K. Hanabusa, L-lysine-based low-molecular-weight gelators, *Chem. Soc. Rev*, **2009**, *38*, 967-975.

[21] T. Kitahara, M. Shirakawa, S. Kawano, U. Beginn, N. Fujita, S. Shinkai, Creation

of a Mixed-Valence State from One-Dimensionally Aligned TTF Utilizing the Self-Assembling Nature of a Low Molecular-Weight Gel, *J. Am. Chem. Soc.*, **2005**, *127*, 14980-14981.

[22] C. Martin, K. Kennes, M. V. Auweraer, J. Hofkens, G. de Miguel, E. M. Garcia-Frutos, Self-Assembling Azaindol Organogel for Light-Emitting Devices (OLEDs), *Adv. Funct. Mater.*, **2017**, n/a.

[23] J.N. Spencer, G. M. Bodner, L. H. Rickard, Chemistry: Structure and Dynamics, Wiley, New York, **2010**.

[24] J. B. Phipps, T. G. Hayes, P. M. Skarstad, D. F. Untereker, In-situ formation of a solid/liquid composite electrolyte in lithium-iodine batteries, *Solid State Ionics*, **1986**, *18-19*, 1073-1077.

[25] J. B. Goodenough, K.-S. Park, The Li-ion Rechargeable Battery: A perspective, *J. Am. Chem. Soc.,* **2013**, *135*, 1167-1176.

[26] M. M. Thackeray, C. Wolverton, E. D. Isaacs, Electrical energy storage for transportation-approaching the limits of, and going beyond, lithium-ion batteries, *Energy Environ. Sci*., **2012**, *5*, 7854-7863.

[27] B. Qiu, X. Zhao, D. Xia, In situ synthesis of CoS2/RGO nanocomposites with enhanced electrode performance for lithium-ion batteries, *J. Alloy Compd.*, **2013**, *579*, 372-376.

[28] E. C. Evarts, Lithium batteries: To the limits of lithium, *Nature*, **2015**, *526*, 93-95.

[29] G. Zheng, S. W. Lee, Z. Liang, H. W. Lee, K. Yan, H. Wang, W. Li, S. Chu, Y. Cui, Interconnected hollow carbon nanospheres for stable lithium metal anodes, *Nanotechnology*, **2014**, *9*, 618-623.

[30] MF. De Volder, SH. Tawfick, RH. Baughman, AJ. Hart, Carbon Nanotubes: Present and Future Commercial Application, *Science*, **2013**, *339*, 535-539.

[31] E. Yoo, J. Kim, E. Hosono, H. S. Zhou, T. Kudo, I. Honma, Large Reversible Li Storage of Graphene Nanosheet Families for Use in Rechargeable Lithium Ion Batteries, *Nano Lett.*, **2008**, *8*, 2277-2282.

[32] M. He, K. Kravchyk, M. Walter, M. V. Kovalenko, Monodisperse Antimony Nanocrystals for High-Rate Li-ion and Na-ion Battery Anodes: Nano versus Bulk, *Nano Lett.*, **2014**, *14*, 1255-1262.

[33] Y. Idota, T. Kubota, A. Matsufuji, Y. Miyasaka, Tin-based amorphous oxide: a high-capacity lithium-ion-storage material, *Science*, **1997**, *276*, 1395-1397.

[34] H. Wu, G. Chan, J. W. Choi, I. Ryu, Y. Yao, M. T. McDowell, S. W. Lee, A. Jackson, Y. Yang, L. Hu, Y. Cui, Stable cycling of double-walled silicon nanotube battery anodes through solid-electrolyte interphase control, *Nature Nanotech.*, **2012,** *7*, 310-315.

[35] U. Kasavajjula, C. Wang, A. J. Appleby, Nano- and bulk-silicon-based insertion anodes for lithium-ion secondary cells, *J. Power Sources*, **2007**, *163*, 1003-1039.

[36] K. Mizushima, P. C. Jones, P. J. Wiseman, J. B. Goodenough, Lithium cobalt oxide(LixCo2)(0<x≤1): a new cathode material for batteries of high energy density, *Mater. Res. Bull.*, **1980**, *15*, 783-789.

[37] T. Ohzuku, R. J. Brodd, An overview of positive-electrode materials for advanced lithium-ion batteries, *J. Power Sources*, **2007**, *174*, 449-456.

[38] W. Zhang, Structure and performance of LiFePO4 cathode materials: A review, *J. Power Sources*, **2011**, *196*, 2962-2970.

[39] N. Yabuuchi, T. Ohzuku, Novel lithium insertion material of LiCo1/3Ni1/3Mn1/3O2 for advanced lithium-ion batteries, *J. Power Sources*, **2003**, *119-121*, 171-174.

[40] Q. Zhong, A. Bonakdarpour, M. Zhang, Y. Gao, J.R. Dahn, Synthesis and electrochemistry of LiNixMn2-xO4, *J. Electrochem. Soc*, **1997**, *144*, 205-213.

[41] D. Liu, J. Hamel-Paquet, J. Trottier, F. Barray, V. Gariepy, P. Hovington, A. Guerfi, A. Mauger, C. M. Julien, J. B. Goodenough, K. Zaghib, Synthesis of pure phase disordered LiMn1.45Cr0.1Ni0.45O4 by a post-annealing method, *J. Power Sources*, **2012**, *217*, 400-406.

[42] A. K. Padhi, K. S. Nanjundaswamy, C. Masquelier, S. Okada, J. B. Goodenough,

Effect of structure on the Fe3+/Fe2+ redox couple in iron phosphates, *J. Electrochem. Soc.*, **1997**, *144*, 1609-1613.

[43] J. B. Goodenough, General Concepts in Lithium Ion Batteries: Fundamentals and Performance, Wiley-VCM, Weinheim, **1998**.

[44] K. Xu, Nonaqueous Liquid Electrolytes for Lithium-Based Rechargeable Batteries, *Chem. Rev.*, **2004**, *104*, 4303-4417.

[45] J. T. Dudley, D. P. Wilkinson, G. Thomas, R. LeVae, S. Woo, H. Blom, C. Horvath, M. W. Juzkow, B. Denis, P. Juric, P. Aghakian, J. R. Dahn, Conductivity of electrolytes for rechargeable lithium batteries, *J. Power Sources*, **1991**, *35*, 59-82.

[46] D. Linden, Handbook of batteries second edition, Mcgraw-hill, New York, **1995**.

[47] Z. Chang, C. Li, Y. Wang, B. Chen, L. Fu, Y. Zhu, L. Zhang, Y. Wu, W. Huang, A lithium ion battery using an aqueous electrolyte solution, *Sci.. Rep.*, **2016**, *6*, 28421.

[48] K. Hanabusa, Electrochemical Aspects of Ionic Liquids part 26, edited by O. Hiroyuki, Wiley & Sons, New Jersey, **2005**.

[49] A. Manthiram, X, Yu, S. Wang, Lithium battery chemistries enable by solid-state electrolyte, *Nature Rev. Mater*., **2017**, *2(3)*, 16103.

[50] M. Faraday, Experimental researches in electricity. Third series, *Phil. Trans. R. Soc. Lond.,* **1833**, *123*, 23-54.

[51] P. G. Bruce, A. R. West, The a.c. conductivity of polycrystalline LISICON, lithium zinc germinate (Li2+2xzn1-xGeO4), and a model for intergranular constriction resistances, *J. Electrochem. Soc.*, **1983**, *130*, 662-669.

[52] K. Murata, S. Izuchi, Y. Yoshihisa, An overview of the research and development of solid polymer electrolyte batteries, *Electrochim. Acta*, **2000**, *45*, 1501-1508.

[53] W. Li, Y. Pang, J. Liu, G. Liu, Y. Wang, Y. Xia, A PEO-based gel polymer electrolyte for lithium ion batteries, *RSC Adv.*, **2017**, *7*, 23494-23501

[54] J. Liu, J. Xu, Y. Lin, J. Li, Y. Lai, C. Yuan, J. Zhang, K. Zhu, All-solid-state Lithium Ion Battery: Research and Industrial Prospects, *Acta Chimica Sinica*, **2013**, *71*, 869-878.

[55] H. Jiang, Y. Zhang, D. Wu, X. Yu, J. Cao, Design and Characterization of High Performance Electrospun Separator for Lithium Ion Battery. *Acta Polymerica Sinica*, **2015**, *11*, 1271-1279.

[56] U. Ali, K.J.B.A. Karim, N.A. Buang, A Review of the Properties and Applications of Poly(Methyl Methacrylate)(PMMA). *Polymer Reviews*, **2015**, *55,* 678-705.

[57] H. S. Choe, B. G. Carroll, D. M. Pasquariello, K. M. Abraham, Characterization of Some Polyacrylonitrile-Based Electrolytes. *Chemistry of Materials*, **1997**, *9*, 369-379.

[58] W. Kubo, T. Kitamura, K. Hanabusa, Y. Wada, S. Yanagida, Quasi-solid-state dye-sensitized solar cells using room temperature molten salts and a low molecular weight gelator. *Chemical Communication*, **2002**, *(4)*, 374-375.

[59] M. Bielejewski, K. Nowicka, N. Bielejewska, J. Tritt-Goc, Ionic conductivity and thermal properties of a supramolecular ionogel made from a sugar-based low molecular weight gelator and a quaternary ammonium salt electrolyte solution, *J. Electrochem. Soc.*, **2016**, *163*, 187-195.

[60] D. Griller, K. U. Ingold, Persistent carbon-centered radicals, *Acc. Chem. Res.*, **1976**, *9*, 13-19.

[61] K. Oyaizu, H. Nishide, Radical polymers for Organic Electronic Devices: A Radical Departure from Conjugated polymers?, *Adv. Mater*. **2009**, *21*, 2339-2344.

[62] Z. Zhelev, R. Bakalova, I. Aoki, K. Matsumoto, V. Gadjeva, K. Anzai, I. Kanno Nitroxyl radicals as low toxic spin-labels for non-invasive magnetic imaging of blood-brain barrier permeability for conventional therapeutics, *Chem. Commun.* **2009**, *(1)*, 53-55.

[63] C. Ysacco, E. Rizzato, M. A. Virolleaud, H. Karoui, A. Rockenbauer, F. Le Moigne, D. Siri, O. Ouari, R. G. Griffin, P. Tordo, Properties of dinitroxides for use in dynamic nuclear polarization (DNP), *Phys. Chem. Chem. Phys.* **2010**, *12*, 5841-5845.

[64] E. L. Dane, B. Corzilius, E. Rizzato, P. Stocker, T. Maly, A. A. Smith, R. G. Griffin,

O. Ouari, P. Tordo, T. M .Swager, Rigid Orthogonal Bis-TEMPO Biradicals with Improved Solubility for Dynamic Nuclear Polarization, *J. Org. Chem.* **2012**, *77*, 1789-1797.

[65] C. S. Wilcox, Effects of tempol and redox-cycling nitroxides in models of oxidative stress, *Pharmacol. Ther.,* **2010**, *126,* 119-145.

[66] Y. Wu, Y. Hirai, Y. Tsunobuchi, H. Tokoro, H. Eimura, M. Yoshio, S. Ohkoshi, T. Kato, Supramolecular approach to the formation of magneto-active physical gels, *Chem. Sci.* **2012**, *3*, 3007-3010.

[67] A. P. Cotrim, F. Hyodo, K. Matsumoto, A. L. Sowers, J. A. Cook, B. J. Baum, M. C. Krishna, J. B. Mitchell, Differential Radiation Protection of Salivary Glands versus Tumor by Tempol with Accompanying Tissue Assessment of Tempol by Magnetic Resonance Imaging, *Clin. Cancer. Res.* **2007**, *13*, 4928-4933.

[68] S. Nakatsuji, K. Aoki, A. Kojoh, H. Akutsu, J. Yamada, M. Karakawa, Y. Aso, Self-Assembling Aryl-Naphthalendiimide Derivatives with a Nitroxide Radical, *Asian J. Org. Chem.* **2013**, *2*, 164-168.

[69] O. L. Lebedev, S. N. Kzazrnovskii, Catalytic oxidation of aliphatic amines with hydrogen peroxide, *Zh. Obshch. Khim*, **1960**, *30*, 1631-1635.

[70] K. Nakahara, S. Iwasa, M. Satoh, Y. Morioka, J. Iriyama, M. Suguro, E. Hasegawa, Rechargeable batteries with organic radical cathodes, *Chem. Phys. Lett.* **2002**, *359*, 351-354.

[71] H. Nishide, S. Iwasa, Y.-J. Pu, T. Suga, K. Nakahara, M. Satoh, Organic radical battery: nitroxide polymers as a cathode-active material, *Electrochim. Acta*, **2004**, *50*, 827-831.

[72] H. Nishide, T. Suga, Organic radical battery, *Electrochem. Soc. Interface* **2005**, *14,* 32-36.

[73] Y. Li, Z. Jian, M. Lang, C. Zhang, X. Huang, Covalently Functionalized Graphene by Radical Polymers for Graphene-Based High-Performance Cathode Materials, *ACS Appl. Mater. Inter.*, **2016**, *8*, 17352-17359.

Chapter 2

Low-Molecular-Weight Gelators Bearing Electroactive Groups as Cathode Materials for Rechargeable Batteries

2.1 Introduction

A substance is a gel, as defined by Flory, if it has a continuous structure which exhibits solid-like rheological behavior, and has macroscopic dimensions that are permanent on the time scale of an analytical experiment [1]. Recently, low molecular weight gelators (LMWGs), which can form supramolecular gels, have attracted great attention mainly because of their unique properties and potential applications as new soft materials. LMWGs have been reported by many excellent reviews and books [2-6]. Non-covalent forces such as hydrogen bonding, van der Waals, π–π stacking, and electrostatic interactions contribute to the self-assembly. LMWGs form various kinds of nanostructures, such as nanofibers, nanoribbons, nanosheets, nanoparticles, helical, and bundle structures. With a suitable solvent choice it is possible to control the LMWGs nanostructures [7].

With growing requirements of renewable energy, the demand for green lithium ion batteries is continuously increasing. The cathode materials generally used in lithium-ion batteries are inorganic materials (e.g., $LiCoO_2$, $LiMnO_4$), which have some drawbacks involving the limited theoretical capacity, unrenewable resources, and large energy consumption. Organic compounds, which can be prepared by environmentally benign processes, have been investigated for renewable resources. Their structures also allow them to be used for several different applications. Organic electroactive materials have some superior advantages, i.e., lightness, flexibility, and processing compatibility.

Nitroxides, as stable organic radicals, represent an interesting class of molecules that form the basis of novel and emerging functional materials such as radical batteries [8], spin probes [9], polarizing agents for DNP-NMR [10,11], antioxidants [12], magneto-active materials [13], and radiation protective agents [14] owing to their single component charge-transfer properties [15]. TEMPO is a persistent radical, which has been protected by four α-methyl groups. The reversible one-electron oxidation leads to the corresponding N-oxoammonium cation $TEMPO^+$. TEMPO and its derivatives are

usually used for controlling the molecular weight in organic polymerization processes. TEMPO also shows redox properties that can be used for rechargeable batteries [16]. The stable nitroxide in poly(2,2,6,6-tetramethylpiperidinyloxy-4-yl methacrylate) (PTMA) presents a flat charge/discharge voltage profile at 3.6 V (vs. Li+/Li) with a theoretical capacity of 111 mA h g^{-1}. PTMA was originally studied as a cathode material by Hasegawa and co-workers [17] in 2002 and further developments have been proposed by Nishide and Suga [18,19]. PTMA exhibits high capacity, high charging and discharging rate performance, and a long cycle life [17].

In this chapter, we describe the gelators containing TEMPO moiety and their remarkable gelation properties in some organic solvents. The morphology test shows the 3D network structure of the xerogel of gelators below the minimum gelation concentration. Electrochemical tests were used to analyze the electrochemical properties. Redox properties and redox voltage were observed by cyclic voltammetry. Output voltage was observed bygalvanostatic tests with an output voltage of 4.8 V.

2.2 Experimental

2.2.1 Material

4-Hydroxy-2,2,6,6-tetramethyl-piperidine 1-oxyl free radical (4-OH TEMPO) and glutaric anhydride were purchased from TCI. Succinic anhydride was purchased from Wako. L-Isoleucylaminooctadecane was prepared by deprotection of the carbobenzyloxy group in *N*-carbobenzyloxy-L-isoleucyaminnooctadocane [20]. All the solvent and materials were used without further purification.

2.2.2 Preparation of samples

The FTIR spectra were measured using a JASCO FS420 with the KBr disc method. Compounds **2a** and **2b** were synthesized by an addition reaction between L-isoleucylaminooctadecane and succinic anhydride or glutaric anhydride.

L-Isoleucylaminooctadecane (3.82 g, 10 mmol) and 1.0 g (10 mmol) of succinic anhydride were dissolved in 200 mL dry CH_2Cl_2 and refluxed overnight, followed by evaporated. Recrystallization from 400 mL of ethyl acetate gave a white product.

2a: Yield: 73%; FTIR (ATR cm^{-1}): 1705 cm^{-1}(υ C=O, –COOH), 1634 cm^{-1}(υ C=O, amide I), 1544 cm^{-1}(δ N–H, amide Ⅱ); Elemental analysis calculated: C 63.13, H 9.71, N 6.14 %; Found: C 62.89, H 9.80, N 6.45 %.

2b: Yield: 72%; FTIR (ATR cm^{-1}): 1705 cm^{-1}(υ C=O, –COOH), 1634 cm^{-1}(υ C=O, amide I), 1544 cm^{-1}(δ N–H, amide Ⅱ); Elemental analysis calculated: C 63.80, H 9.85, N 5.95 %; Found: C 63.54, H 9.81, N 6.04 %.

Compounds **3a** and **3b** were synthesized by a coupling reaction between 4-OH TEMPO and **2a**/**2b**. A mixture of 2.75 g (16 mmol) of 4-OH TEMPO, 7.7 g (16 mmol) of **2a**, 2.21 g (17.6 mmol) of DIPC (*N,N'*-diisopropylcarbodiimide), and 4.9 g (17.6 mmol) of DPTS (4-dimethylamino pyridinium *p*-toluenesulfonate) in 50 mL of dry CH_2Cl_2 were refluxed overnight at 50°C. After the solvents were evaporated, the product was first recrystallized using 30 mL of THF and then with 20 mL of methanol to remove the catalyst. Finally, recrystallization from 20/400 mL of dichloromethane/ether gave an orange product.

3a: Yield: 53%; FTIR (ATR cm^{-1}): 1736 cm^{-1}(υ –COO–), 1634 cm^{-1}(υ C=O, amide I), 1544 cm^{-1}(δ N–H, amide Ⅱ); Elemental analysis calculated: C 69.70, H 11.08, N 6.60 %; Found: C 69.23, H 11.31, N 6.67 %; m.p. = 81°C.

3b: Yield: 55%; FTIR (ATR cm^{-1}): 1736 cm^{-1}(υ –COO–), 1634 cm^{-1}(υ C=O, amide I), 1544 cm^{-1}(δ N–H, amide Ⅱ); Elemental analysis calculated: C 72.17, H 11.49, N 6.47 %; Found: C 71.04, H 11.45, N 6.57 %; m.p. = 78°C.

2.2.3 Gelation experiments

A gelation test was performed using a test tube with the compound and organic solvent inside. A sample was dissolved in a solvent by heating and then cooled to

25 °C for 2 h. The gel formation was recognized visually by the test tube upside-down method.

2.2.4 AFM observation

Atomic force microscopy (AFM) was performed on a SPA-4001 from SⅡ Company. A 1-cm length square mica plate was put on the AFM test metal sheet with correction fluid between them to adhere them. The sample was prepared below the minimum gelation concentration. Then, one drop of the solution was dropped on the mica plate. After spin-coating, the mica plate was dried under vacuum over two nights.

2.2.5 TEM observation

Transmission electron microscopy (TEM) was observed on a JEOL-2010 electron microscope at a voltage of 200 kV. A sample was prepared below the minimum gelation concentration, and then dropped on the grid with a carbon film. After drying in a vacuum for 2–3 days, the sample was stained with osmium tetroxide over one night.

2.2.6 Electrochemical procedure

The electrochemical spectra were measured using a Solartron SI 1287 electrochemical interface from TOYO Corporation.

Gel form: A 0.27-cm-thick Teflon plant with a hole radius of 0.3 cm, was adhered with insulation tape on both sides. Compound of 50 mg was dissolved in 1 mL γ-butyrolactone (γ-BL) with 1M electrolyte of $LiBF_4$, after heating, filled in the hole of the Teflon plant. The Teflon plant was then sandwiched between two pieces of ITO electrodes and placed in an oven at 25 °C for 2 hours.

Xerogel form: A compound was dissolved in an organic solvent and dropped on the ITO electrodes. The sample was then dried under vacuum for 2–3 days.

2.3 Results and Discussion

2.3.1 Gelation properties

A gel is a kind of soft material which not only has outstanding physical properties like metals but also has excellent chemical characteristics like liquid. To form a gel, it is necessary to focus on the force between the molecules, which make such amazing products. Hydrogen bonding, van der Waals, π–π stacking, electrostatic interactions, and other interaction forces contribute to 3D network structures of gels.

Gelators containing TEMPO were synthesized by the coupling reaction between gelation-driving segments (**2a** or **2b**) and 4-OH TEMPO (Figure 2.1).

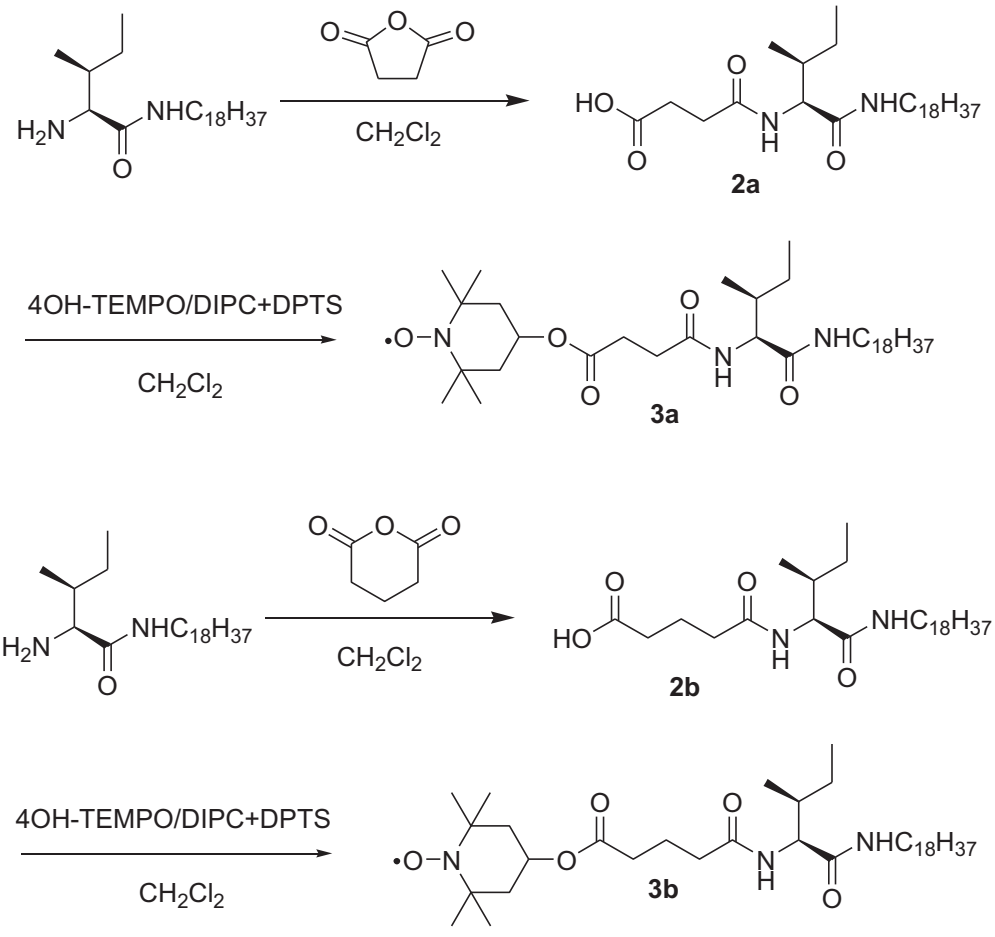

Figure 2.1 Synthesis of **3a** and **3b**.

Table 2.1 shows the results of the gelation tests. The compounds **3a** and **3b** showed superior gelation ability in γ-Butyrolactone (γ-BL) and propylene carbonate (PC), which were widely used as an electrolyte solution in batteries because of their high boiling point, low melting point, high flash point, and high conductivity. The compounds also formed gels in some polar solvents such as methanol and DMF. The major gelation driving force for the amide derivatives is the H-bonding. For our compounds, the predicted molecular-packing structure of the compounds is shown in Figure 2.2, where the H-bonding between the NH and CO groups makes the solution form a gel. The photographs of solutions and gels of **3a** are shown in Figure 2.3.

Table 2.1 Results of the gelation tests of **3a** and **3b** for typical solvents at 25°C.

Solvent	**3a**	**3b**
Methanol	GTL(40)	GO(20)
Ethanol	PG	PG
1-Propanol	S	PG
Acetone	I	I
THF	S	S
Ethyl acetate	I	GO(20)
DMF	S	GO(20)
Toluene	S	S
Chloroform	S	S
γ-Butyrolactone	GTL(5)	GTL(4)
Propylene Carbonate	GTL(5)	GTL(4)

GO: Opaque gel, GTL: Translucent gel, GT: Transparent gel S: Solution at 40 mg mL^{-1}, PG: partial gel at 40 mg mL^{-1} I: Insoluble at 40 mg mL^{-1}

The gelation process of the LMWGs is as follows: at first, through non-covalent forces such as H-bonding, the molecules self-assembled and formed fibrous aggregates,

which eventually turned into a 3D network that immobilized the solvent molecules. Nano-sized fibrous aggregates can be easily observed using an electron microscope, which will be introduced later.

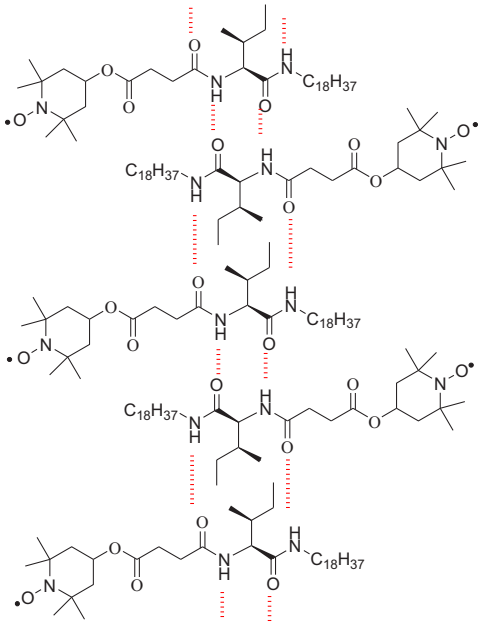

Figure 2.2 Structure of the gel aggregate

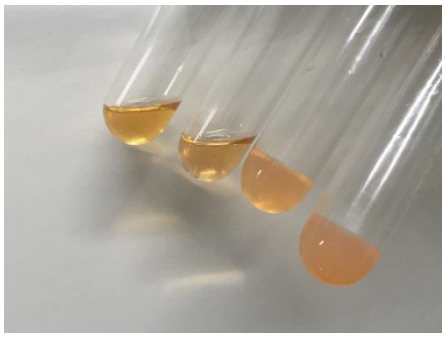

Figure 2.3 Photographs of samples. The solvents are chloroform (solution), DMF (solution), PC (gel), and γ-BL (gel) from right to left.

2.3.2 Morphology of supramolecular gel

The supramolecular aggregates formed in the gel phase were further characterized

and studied using AFM and TEM. Figure 2.4 and Figure 2.5 shows typical TEM and AFM images of the fibrous aggregates in the gel at a concentration of 1 mg mL^{-1} of **3a** or **3b** in PC. In both AFM images, fibrous aggregates could be easily observed, and the diameters of the fibers was in the range of 20–50 nm. There were several crude fibers with diameters above 100 nm, which was caused by the inhomogeneous state while drying. The TEM images also showed the same shapes as observed in the AFM images. All the gels formed were made by the fibrous aggregates which were built by H-bonding between the molecules.

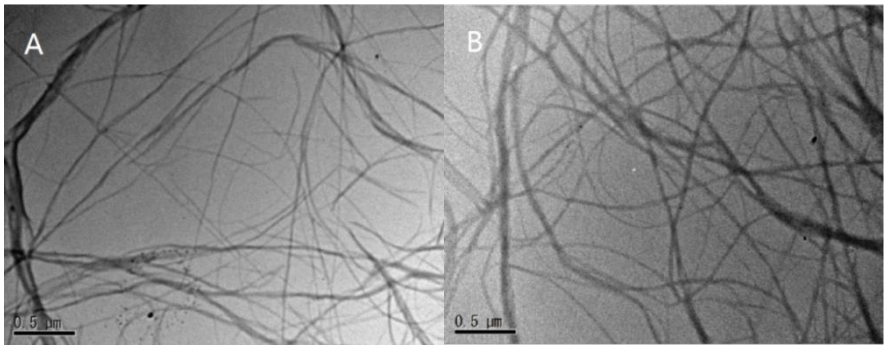

Figure 2.4TEM images of **3a** (A) and **3b** (B) xerogels prepared from a solution of 1 mg mL^{-1}. The scale bars are 500 nm.

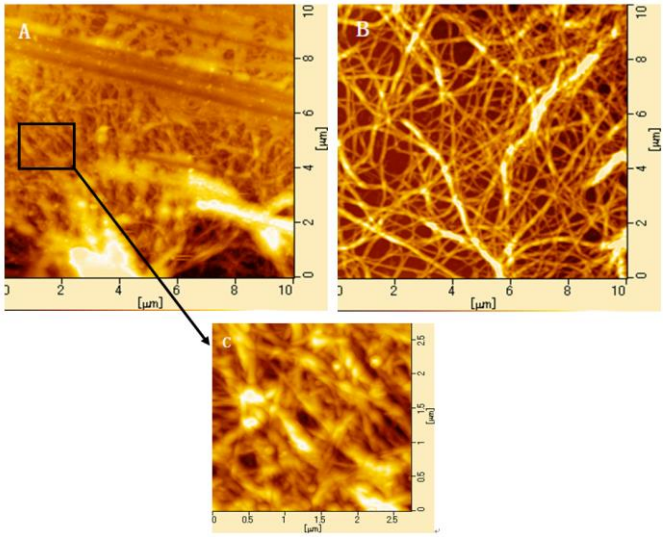

Figure 2.5 AFM spectra of **3a** and **3b**. (A) **3a** at 1 mg mL^{-1}; (B) **3b** at 1 mg mL^{-1}; (C) zoomed region image of (A)

2.3.3 Electrochemical properties of 3a and 3b

Figure 2.6 shows redox of TEMPO and $TEMPO^+$. The cyclic voltammograms (CVs) were obtained to measure the redox properties of **3a** and **3b**. Because the similar results were observed for both compounds, we will discuss the result of sample **3a**. To investigate the oxidation and reduction properties of the compounds, we tested the charging and discharging at different voltage ranges (Figure 2.7). In the range of 0 V to -1 V, no cathode and anode peaks were observed (Figure 2.7(A)) and in the range of 0 V to 1 V, an unambiguous peak was observed (Figure 2.7(B)). When the voltage range was expanded to -1 V to 1 V, the oxidation peak for the radical during the voltage increase and the reduction peak during the voltage decrease were observed (Figure 2.7(C)). Compared with the CV results of the gel formed with the raw material 4OH-TEMPO and **2a** (Figure 2.7(D)), the same oxidation and reduction voltages were observed. It shows that the electrochemical activities of the radical in the gel made by **2a** and in the gel made by **3a** with the radical were approximately identical. For the CV experiment, the oxidation peak of the first cycle was smaller than others because of the form of the solid electrolyte interface (SEI film) and its thermal oxidation during synthesis and manufacturing.

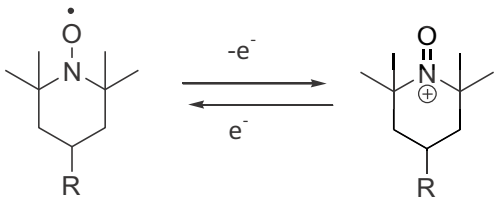

Figure 2.6 Redox of TEMPO and $TEMPO^+$

We also obtained the linear relationship between I_a and scan rate for these systems. The linear plots can be used to determine the diffusion coefficient (D) of the electroactive species, TEMPO, by using the Randles-Sevcik equation [21]. This equation relates the value of the anodic peak current I_p for one electron reversible

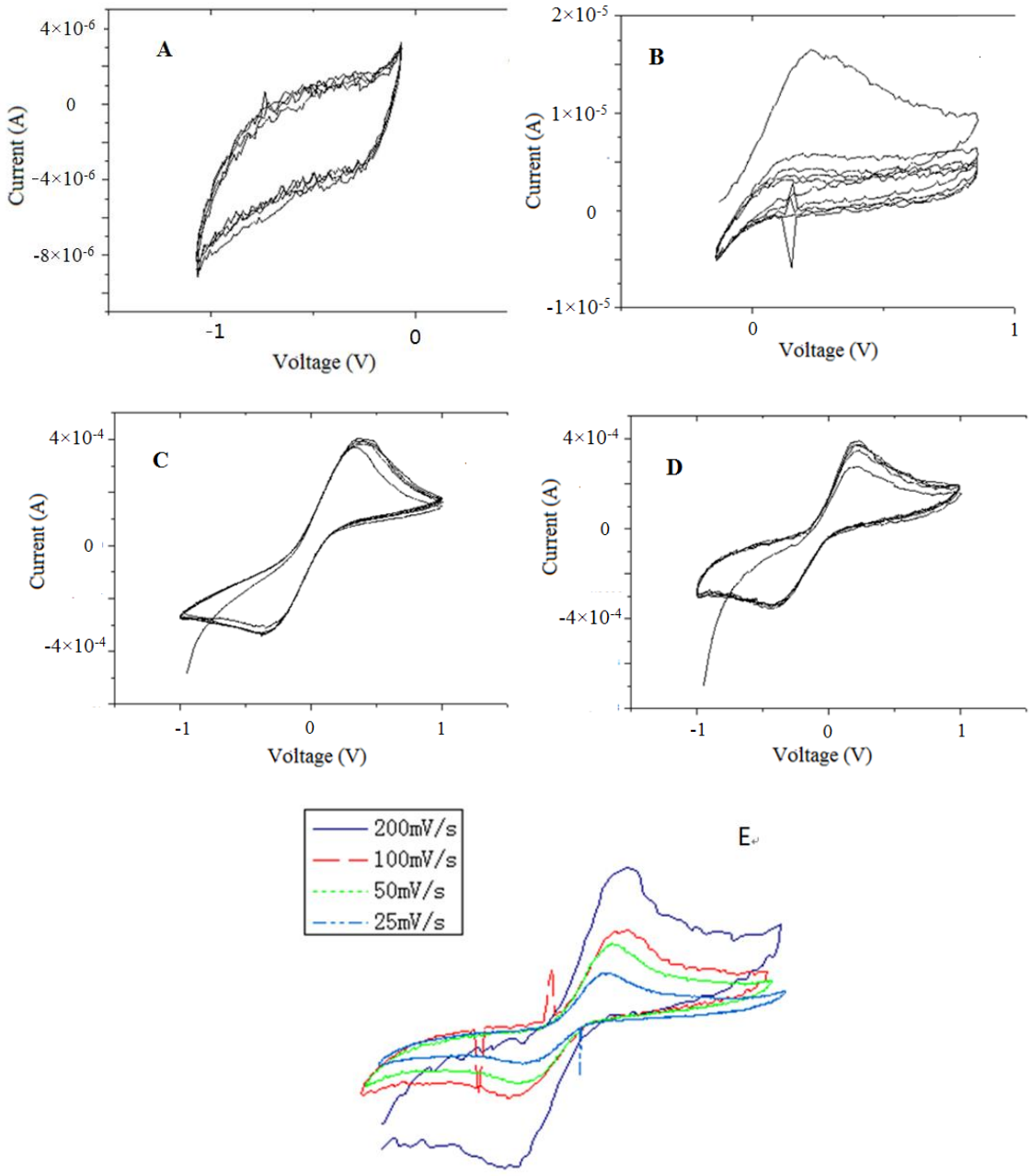

Figure 2.7 Cyclic Voltammograms of **3a** and raw material at 25 °C:(A) -1V–0V, gel form of 50 mg mL^{-1} **3a**, 200mV/s (B)0V–1V, gel form of 50 mg mL^{-1} **3a**, 200mV/s, (C) -1V–1V, gel form of 50 mg mL^{-1} **3a**, 200mV/s (D) -1V–1V, gel form of 50 mg mL^{-1} **2a** and 4-OH TEMPO, 200mV/s (E) different scan rates of gel of 50 mg mL^{-1} **3a** from -1V to 1V.

process to the scan rate and *D* through the following equation:

$$i_p = 0.4463\ nFAC\left(\frac{nFvD}{RT}\right)^{\frac{1}{2}}$$

Eq. (1)

Where *A* is the area of the electrode, F is the Faraday's constant, *C* is the concentration of the electroactive species, and other parameters have their usual meanings. The prediction of this equation that I_p increases at faster voltage scan rates appears counterintuitive. It is important to remember that current, *I*, is charge (or electrons) passed per unit time. Therefore, at faster voltage scan rates, the charge passed per unit time is greater, hence an increase in I_P. While the total amount of charge was the same [22], we also notice that with increasing scan rate the oxidation peak also increased, which is probably caused by the polarization and the IR drop.

To the best of our knowledge, there is no paper that discusses the influence of the gel concentration on the electrochemical active properties. We have measured gel samples of different concentrations (Figure 2.8). A decreased oxidation current was observed with increased concentration of the gelator when comparing the samples prepared with gelator concentration of 50 mg mL^{-1} and 100 mg mL^{-1}. We predict that with increasing concentration the fibers become more concentrated, and the gap between the fibers becomes smaller, and that makes it difficult for Li^+ ions to move through the gel form. So even if the concentration is increased, the oxidation current might decrease.

We also measured the CV of the xerogel of our samples (Figure 2.9). The oxidation and reduction peaks of the xerogel made from the raw material 4-OH TEMPO and **2a** were difficult to characterize, whereas the **3a** xerogel showed clear peaks and redox properties. This suggests that in the xerogel form, the electronic activities of our compounds are greater than the raw material and gelator **2a**.

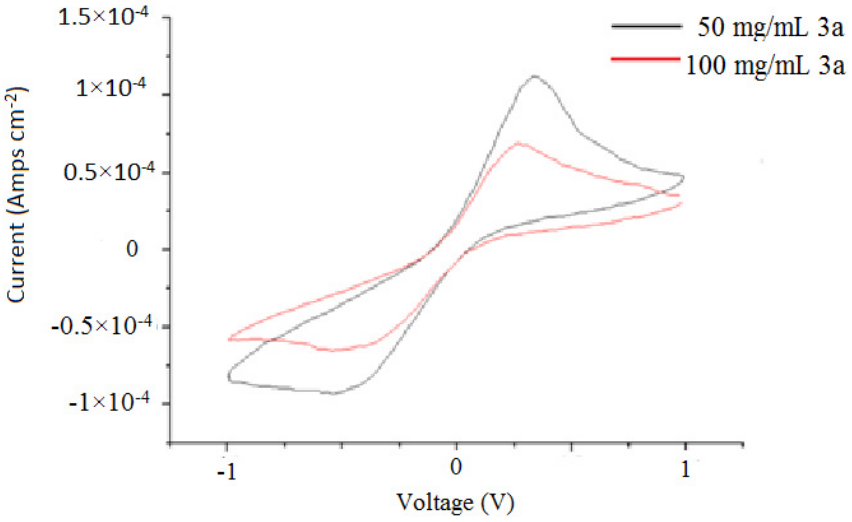

Figure 2.8 Cyclic Voltammograms of 50mg mL^{-1} and 100mg mL^{-1} **3a** gel

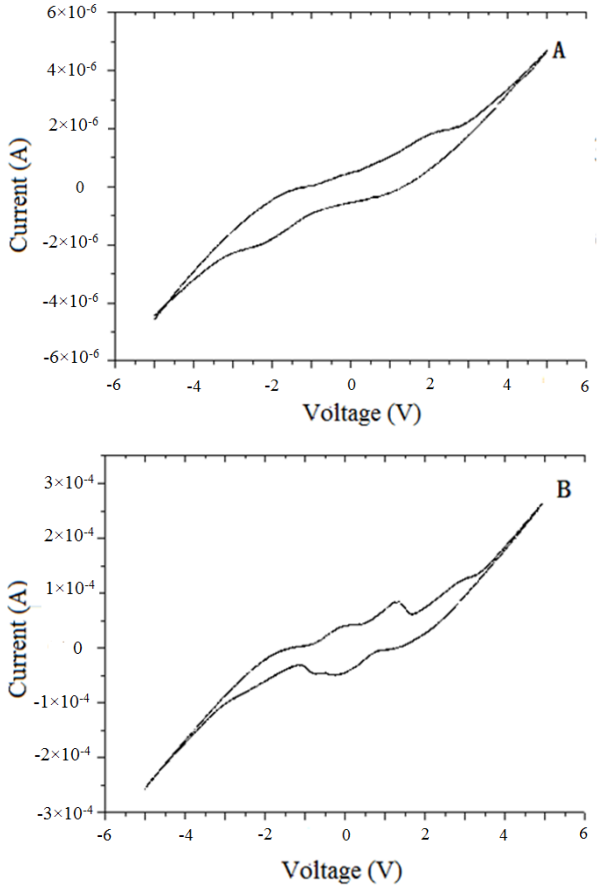

Figure 2.9 Cyclic voltammograms of xerogel: (A) **2a** and 4-OH TEMPO (B) **3a**

The output voltage of 50 mg mL^{-1} **3a** sample is about 4.8 V at the charge/discharge current of 10^{-4} A cm^{-2} for 100 seconds (Figure 2.10), which suggests that our compounds can be used for high voltage energy storage devices.

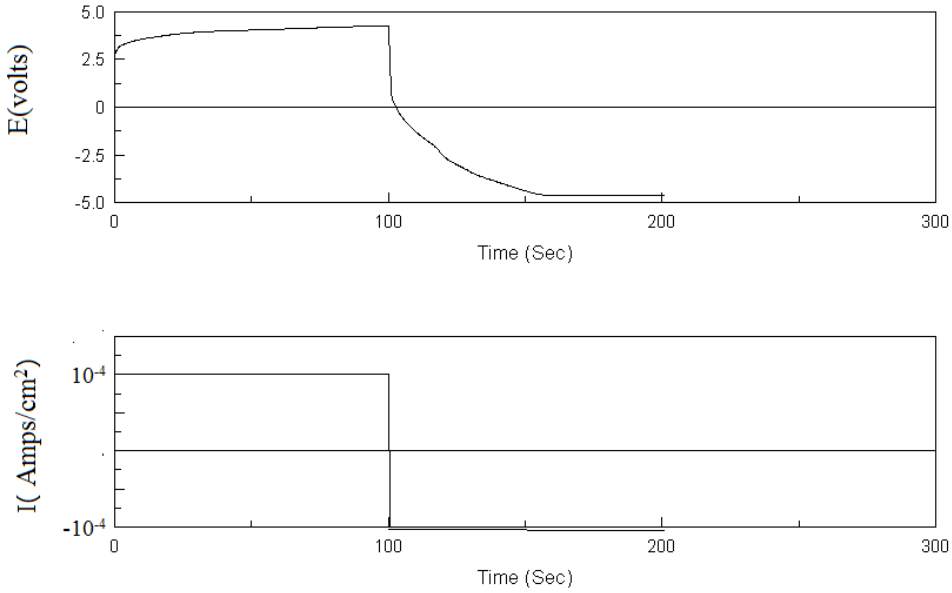

Figure 2.10 Galvanostatic test of sample **3a**

2.4 Conclusion

We synthesized two compounds that have a nitroxide radical and a gelation driving segment, and investigated their gelation abilities and electrochemical properties. AFM and TEM showed that our samples were 3D network of fibrous aggregates that immobilized the solvent molecules. The redox properties of our compounds showed that the electroactivity of the xerogel was much higher than that of the raw material. However, with the increasing of the concentration, the close network structure might obstruct the movement of Li^+ ions and hinders its redox properties. With these characteristics, our compounds may have excellent performance in energy storage devices.

2.5 References

[1] P.J. Flory, Gels and gelling process. *Faraday Discuss. Chem. Soc.*, **1974**, *57*, 7-18.

[2] P. Terech. R. G. Weiss, Low Molecular Mass Gelators of Organic Liquids and Properties of Their Gels, *Chem. Rev.* **1997**, *97*, 3133-3160.

[3] L. A. Estroff, A. D. Hamilton, Water Gelation by Small Organic Molecules, *Chem. Rev.* **2004**, *104*, 1201-1217.

[4] N. Sangeetha, U. Maitra, Supramolecular gels: Functions and uses, *Chem. Soc. Rev.* **2005**, *34*, 821-836.

[5] M. de Loos, B. L. Feringa, J. H. van Esch, Design and Application of Self-Assembled Low Molecular Weight Hydrogels, *Eur. J. Org. Chem.* **2005**, *17*, 3615-3631.

[6] R. G. Weiss and P. Terech, *Molecular Gels: Materials with Self-assembled Fibrillar Networks*, Springer, Dordrecht **2006.**

[7] M. Suzuki, K. Hanabusa, L-Lysine-based low-molecular-weight gelators, *Chem. Soc. Rev.* **2009**, *38*, 967-975.

[8] (a) K. Oyaizu, H. Nishide, Radical polymers for Organic Electronic Devices: A Radical Departure from Conjugated polymers?, *Adv. Mater*. **2009**, *21*, 2339-2344.
(b) T. Janoschka, M. D. Hager, U. S. Schubert, Powering up the Future: Radical Polymers for Battery Applications, *Adv. Mater.* **2012**, *24*, 6397-6409.

[9] Z. Zhelev, R. Bakalova, I. Aoki, K. Matsumoto, V. Gadjeva, K. Anzai, I. Kanno, Nitroxyl radicals as low toxic spin-labels for non-invasive magnetic imaging of blood-brain barrier permeability for conventional therapeutics, *Chem. Commun.* **2009**, *(1)*, 53-55.

[10] C. Ysacco, E. Rizzato, M. A. Virolleaud, H. Karoui, A. Rockenbauer, F. Le Moigne, D. Siri, O. Ouari, R. G. Griffin, P. Tordo, Properties of dinitroxides for use in dynamic nuclear polarization (DNP), *Phys. Chem. Chem. Phys.* **2010**, *12*, 5841-5845.

[11] E. L. Dane, B. Corzilius, E. Rizzato, P. Stocker, T. Maly, A. A. Smith, R. G. Griffin, O. Ouari, P. Tordo, T. M. Swager, Rigid Orthogonal Bis-TEMPO Biradicals with Improved Solubility for Dynamic Nuclear Polarization, *J. Org. Chem.* **2012**, *77*, 1789-1797.

[12] C. S. Wilcox, Effects of tempol and redox-cycling nitroxides in models of oxidative stress, *Pharmacol. Ther.,* **2010**, *126,* 119-145.

[13] Y. Wu, Y. Hirai, Y. Tsunobuchi, H. Tokoro, H. Eimura, M. Yoshio, S. Ohkoshi, T. Kato, Supramolecular approach to the formation of magneto-active physical gels, *Chem. Sci.* **2012**, *3*, 3007-3010.

[14] A. P. Cotrim, F. Hyodo, K. Matsumoto, A. L. Sowers, J. A. Cook, B. J. Baum, M. C. Krishna, J. B. Mitchell, Differential Radiation Protection of Salivary Glands versus Tumor by Tempol with Accompanying Tissue Assessment of Tempol by Magnetic Resonance Imaging, *Clin. Cancer. Res.* **2007**, *13*, 4928-4933.

[15] S. Nakatsuji, K. Aoki, A. Kojoh, H. Akutsu, J. Yamada, M. Karakawa, Y. Aso, Self-Assembling Aryl-Naphthalendiimide Derivatives with a Nitroxide Radical, *Asian J. Org. Chem.* **2013**, *2*, 164-168.

[16] T. Sukegawa, K. Sato, K. Oyaizu, H. Nishide, Efficient charge transport of a radical polyether/SWCNT composite electrode for an organic radical battery with high charge-storage density, *RSC Adv.*, **2015**, *5*, 15448-15452.

[17] K. Nakahara, S. Iwasa, M. Satoh, Y. Morioka, J. Iriyama, M. Suguro, E. Hasegawa, Rechargeable batteries with organic radical cathodes, *Chem. Phys. Lett.* **2002**, *359*, 351-354.

[18] H. Nishide, S. Iwasa, Y.-J. Pu, T. Suga, K. Nakahara, M. Satoh, Organic radical battery: nitroxide polymers as a cathode-active material, *Electrochim. Acta*, **2004**, *50*, 827-8331.

[19] H. Nishide, T. Suga, Organic radical battery, *Electrochem. Soc. Interface* **2005**, *14,* 32-36.

[20] K. Hanabusa, K. Hiratsuka, M. Kimura, H. Shirai, Easy Preparation and Useful

Character of Organogel Electrolytes Based on Low Molecular Weight Gelator, *Chem. Mater.* **1999**, *11*, 649-655.

[21] P. T. Kissinger, W.R. Heineman, Cyclic voltammetry experiment, *J. Chem. Educ.* **1983**, *60*, 772-776.

[22] R. K. Mahajan, N. Kaur, M. S. Bakshi, Cyclic voltammetry investigation of the mixed micelles of conventional with L64 and F127, *Colloid. Surf. A- Physicochem. Eng. Asp.,* **2006**, *276*, 221-227.

Chapter 3

Easy preparation of graphite-containing gel electrolytes using a gelator and characterization of their electrochemical properties

3.1 Introduction

According to the definition by Flory, a substance is a gel if it has a continuous structure that exhibits rheological behavior like a solid and has permanent macroscopic dimensions throughout the duration of an analytical experiment [1]. Gels can be classified into two types, chemical and physical gels. Chemical gels are generally characterized by a three-dimensional (3D) network structure with covalent bonds, and the most distinguished examples of chemical gels are superabsorbent polymers and soft contact lenses. Physical gels are characterized by dynamic cross-links that are constantly created and broken so that the gel changes its state between solid and liquid under the influence of environmental factors [2]. Low-molecular-weight gelators (LMWGs) have captured great attention because of their singular properties and potential applications as soft materials in several fields. LMWGs, which have been reported by many outstanding books and reviews [3–7], usually form self-assembled gels through noncovalent forces such as hydrogen bonding, van der Waals force, π–π stacking, and electrostatic interactions. LMWGs can comprise numerous nanostructures, such as nanofibers, nanoribbons, nanosheets, nanoparticles, helices, and bundle structures. In this regard, LMWGs are characterized by their ability to form several types of nanostructure in suitable solvents [8].

A key component in lithium-ion batteries is the electrolyte. Traditional lithium-ion batteries use polar solvents and lithium ions as the electrolyte, thus providing advantages such as high conductivity, low cost, high ion transport speed, and long cycle life. However, some challenges, such as leakage and inflammability, exist that limit their possible applications. Solid electrolytes have also played an important role in solid-state batteries because they offer higher energy density than traditional electrolytes in normal lithium-ion batteries. However, the problems of stability, mechanical strength, cost, and environmental influences have not yet been solved satisfactorily. With regard to the shortcomings of traditional electrolytes, gel electrolytes have been widely studied.

Gel electrolytes are materials that combine the properties of both liquid and solid electrolytes. They do not contain an inflammable liquid electrolyte and thus can improve the safety performance of lithium-ion batteries while providing the conductivity of liquid electrolytes [9–13]. As they exhibit a conductivity similar to that of liquid electrolytes, many gel polymers such as poly(ethylene oxide) [9, 14], poly(vinylidene fluoride) [10], poly(methyl methacrylate) [11, 12], and polyacrylonitrile [13] have been widely reported. Apart from these, some LMWGs have been used to convert liquid electrolytes for lithium-ion batteries to gel via the formation of 3D fibrous networks through intermolecular interactions such as hydrogen bonding and van der Waals force. For example, Yanagida et al. used 1-hexyl-3- -methylimidazolium iodide, iodine, and an L-isoleucine-based LMWG to fabricate quasi-solid-state dye-sensitized solar cells (DSCs) with high stability and good performance [15]. Sun et al. synthesized 1,3:2,4-di-O-dimethylbenzylidene-D-sorbitol prepared from D-sorbitol and 3,4-dimethylbenzaldehyde, which formed a gel with good charge–discharge characteristics in KOH aqueous solution [16]. Basrur et al. combined 1,3:2,4-di-O-methylbenzylideneD-sorbitol as an LMWG with fumed silica to prepare a gel electrolyte using $LiClO_4$ and propylene carbonate (PC) [17]. Li et al. reported a series of LMWGs of N-Boc-D-glutamic ester derivatives that can gel the commercial liquid electrolyte for lithium-ion batteries and broaden their electrochemical window [18].

In this chapter, we focused on L-β-3,7-dimethyloctylasparaginyl-L-phenylalanyl (19) as a LMWG, which were able to synthesize gels with ionic liquids as well as organic solvents. We prepared gels using 1-butyl-3-methylimidazolium tetrafluoroborate ((bmim)BF_4), propylene carbonate (PC), and γ-butyrolactone (γ-BL) in 1 M $LiBF_4$, which contained graphite as a helper additive. Gelation behavior, gel strengths, thermal stabilities, and electrochemical properties of the gel electrolytes were studied with regard to the effect of graphite.

3.2 Experimental

3.2.1 Material

Cyclo(L-β-3,7-dimethyloctylasparaginyl-L-phenylalanyl) was prepared according to the literature [19]. PC and $LiBF_4$ were purchased from TCI. Graphite, γ-BL, and $(bmim)BF_4$ were from purchased Wako Pure Chemical Ltd.

3.2.2 Gelation evaluation

The gelation test was performed using a test-tube upside-down method. A sample was dissolved in a solvent by heating and then the mixture was cooled to 25 °C for 2 h in a temperature-controlled chamber. When no fluid ran down the wall of the test tube upon inversion of the tube, we judged it to be a gel.

3.2.3 TEM observations

Transmission electron microscopy (TEM) was performed using a JEOL-2010 electron microscope at a voltage of 200 kV. The samples were prepared at a concentration below the minimum gelation concentration, and then dropped on a grid that had a carbon film attached to it. After drying in vacuum for 2–3 days, the samples were stained with osmium tetroxide over one night.

3.2.4 Electrochemical measurements

Ionic conductivity and cyclic voltammograms (CVs) were measured using a Solartron SI 1287 electrochemical interface from TOYO Corporation. A 0.27-cm-thick Teflon plant with a hole radius of 0.3 cm was adhered with insulation tape on both sides. The gelator was dissolved in 1 mL of PC or γ-BL dissolved in 1 M $LiBF_4$, and a weighed portion of graphite was added. After heating, the sample was filled in the hole of the Teflon plant. The Teflon plant was then sandwiched between two pieces of ITO electrodes and placed in an oven at 25 °C for 2 h.

3.3 Results and discussion

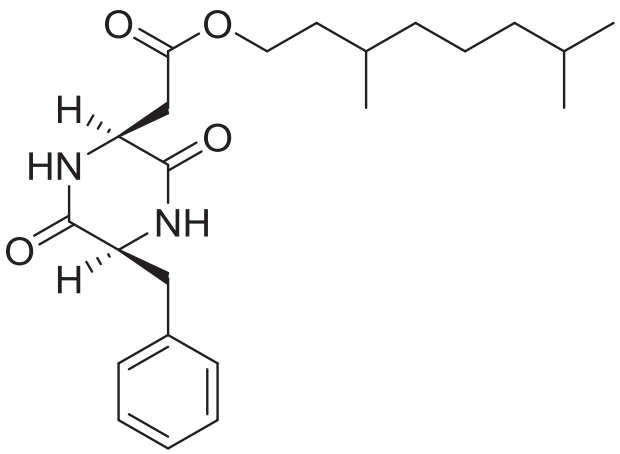

Figure 3.1 Chemical structure of gelator **1.**

3.3.1 Gelation behavior

Strong gelation abilities have so far been found in a family of amino-acid derivatives, and the application of these substances in gel electrolytes was reported [20]. In this study, we studied cyclo(L-β-3,7-dimethyloctylasparaginyl-L-phenylalanyl) (**1**) (Figure 3.1) because (a) it can be easily prepared in moderate yield from "aspartame," which is an artificial sweetener and (b) it can gel most ionic liquids [19] as well as high polar solvents [21]. We studied the gelation behavior of graphite-containing (bmim)BF_4, $LiBF_4$/PC, and $LiBF_4$/γ-BL. The results of the gelation tests are summarized in Table 3.1. One-milliliter samples of solutions containing the sole components (bmim)BF_4, PC, and γ-BL without graphite were gelled by adding 10, 10, and 40 mg, respectively, of gelator **1**. In contrast, solutions of 1 M $LiBF_4$/PC and 1 M LiB_F4/γ-BL could not be gelled even by adding 100 mg of **1**. This result can be explained by the increasing dielectric constants of PC and γ-BL by adding $LiBF_4$. Although we failed in gelling 1 M $LiBF_4$/PC and 1 M $LiBF_4$/γ-BL, we succeeded in gelling them using graphite (particle size ~45 μm) as a helper additive. Figure 3.2 shows photos of the gels of graphite-containing $LiBF_4$/PC prepared by cooling the warm solutions of 1 M LiBF4/PC containing graphite and 100 mg of **1** under ultrasonic irradiation. Notably,

ultrasonic irradiation was indispensable for the formation of gels with homogeneously dispersed graphite. Figure 3.2 also shows the appearance of a precipitate from the solution of 1 M $LiBF_4$/PC containing 100 mg of **1**. The precipitation of **1** from $LiBF_4$/PC and $LiBF_4$/γ-BL suggests that there is a delicate balance between gelation and crystallization. The reason for this is that both gelation and crystallization occur as a result of cooperating non-covalent interactions such as hydrogen bonding and van der Waals forces. The progression from small aggregates of **1** to crystal-like large ones is assumed to accelerate in high polar solvents containing $LiBF_4$. Dispersed graphite in $LiBF_4$/PC and $LiBF_4$/γ-BL prevents this excessive aggregation and consequently forms stable gels.

IR spectra provide important information on hydrogen-bond formation. We measured the FTIR spectra of precipitates from a solution of $LiBF_4$/PC, a gel of PC, a gel of graphite-containing $LiBF_4$/PC, and a chloroform isotropic solution of **1**. In the spectrum of the precipitate, PC gel, and graphite-containing gel, the band at 3329 cm^{-1} was assigned to N–H hydrogen-bonding stretching vibrations. In contrast, the spectrum of the isotropic solution of **1** in chloroform showed N–H stretching vibration at 3382 cm^{-1}, which indicates no hydrogen bonding. The FTIR results suggest that hydrogen bonding among amide plays a vital role in the gelation process regardless of the presence of graphite, and hydrogen bonding works as a driving force for both precipitation and gelation.

The effect of graphite on the 3D networks formed by **1** was studied by TEM. Figure 3.3 shows the TEM images of the PC gels with graphite and graphie-containing PC gels former by **1**; they show fine thread-like aggregates with nearly homogeneous diameters. The aggregate diameters for the PC gel without graphite (Figure 3.3 (a)) and for those containing 2.5 mg/mL graphite (Figure 3.3 (b)) were ~150 nm. However, when 10 mg of graphite was added to 1 mL of PC, the diameter decreased to ~50 nm (Figure 3.3 (c)). We expect that the dispersed graphite in $LiBF_4$/PC and $LiBF_4$/γ-BL works as a wall, preventing excessive aggregation so that slender fibers are formed.

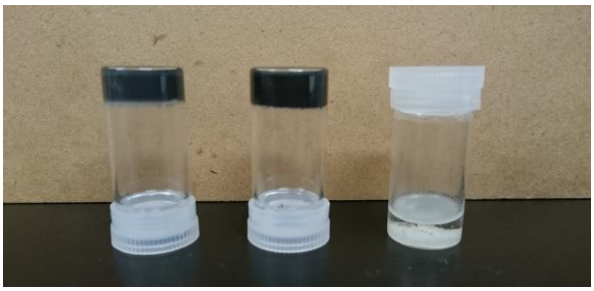

Figure 3.2 Photos of gels and precipitation.

Left; gel prepared from 1 M $LiBF_4$/PC containing graphite and 10 mg of graphite and 100 mg of **1**.

Middle; gel prepared from 1 M $LiBF_4$/PC containing graphite and 100 mg of graphite and 100 mg of **1**.

Right; precipitation from 1 M $LiBF_4$/PC containing 100 mg of **1**.

Table 3.1 Results of gelation test at 25°C.

solvent (1 mL)	gelator **1**/mg	graphite/mg	state
(bmim)BF_4	10	0	opaque gel
PC	10	0	translucent gel
γ-BL	40	0	translucent gel
1 M $LiBF_4$/PC	100	0	precipitation
1 M $LiBF_4$/γ-BL	100	0	precipitation
(bmim)BF_4	10	10–200	opaque gel
PC	10	10–200	opaque gel
γ-BL	40	10–200	opaque gel
1 M $LiBF_4$/PC	100	10–200	opaque gel
1 M $LiBF_4$/γ-BL	100	10–200	opaque gel

(bmim)BF_4: 1-Butyl-3-methylimidazolium tetrafluoroborate, PC: Propylene carbonate, γ-BL: γ-Butyrolactone. The amounts of all solvents were fixed to 1 mL and the concentration of $LiBF_4$ was 1.0 M. The addition amounts of graphite were 10, 50, 100, or 200 mg.

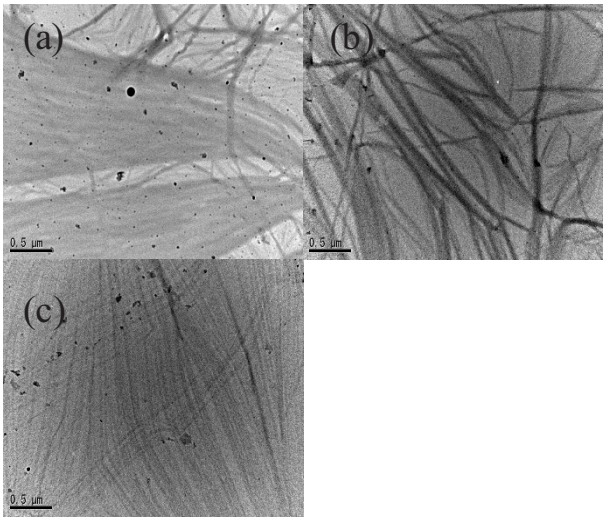

Figure 3.3 TEM images of PC gels.

(a); gel prepared from 5 mg of **1** and 1 mL of PC.

(b); gel prepared from 2.5 mg of graphite, 5 mg of **1**, and 1 mL of PC.

(c); gel prepared from 10 mg of graphite, 5 mg of **1**, and 1 mL of PC.

3.3.2 Gel strength and thermal stability

Gel strength, which is an important parameter in gel applications, is often evaluated by measuring the elastic storage modulus G′ and loss modulus G″. However, in this study, we evaluated the gel strength as the force required to sink a cylindrical bar (10 mm in diameter) 4-mm deep in the gels. In general, gel strength increases nearly in proportion to the added amount of gelator [19, 20]. Increasing the gel strength was also observed in the PC gels prepared using **1** (Figure 3.5); for instance, the strengths of PC gels prepared at 20 and 100 mg/mL (**1**/PC) were ca. 250 and 4160 g cm^{-2} at 25° C, respectively. The trend of increasing the gel strength with increasing gelator amount is reasonable because a higher concentration of **1** would lead to the formation of dense 3D networks.

The gel strengths of graphite-containing (bmim)BF_4, PC, and $LiBF_4$/PC gels were plotted against the amount of graphite added (Figure 3.4). The gel strength of graphite-containing (bmim)BF_4, comprising 50 mg of **1** and 1 mL of (bmim)BF_4, was

more than 1700 g cm^{-2} and increased slightly with increasing amount of graphite. The graphite-containing PC gels prepared from 100 mg of **1** and 1 mL of PC were very hard, and their strength was higher than 3600 g cm^{-2}. In contrast, the strength of the graphite-containing $LiBF_4$/PC gels was very low (~1000 g cm^{-2}) even when 200 mg of graphite was added. This suggests that the addition of graphite only had a slight effect on gel strength.

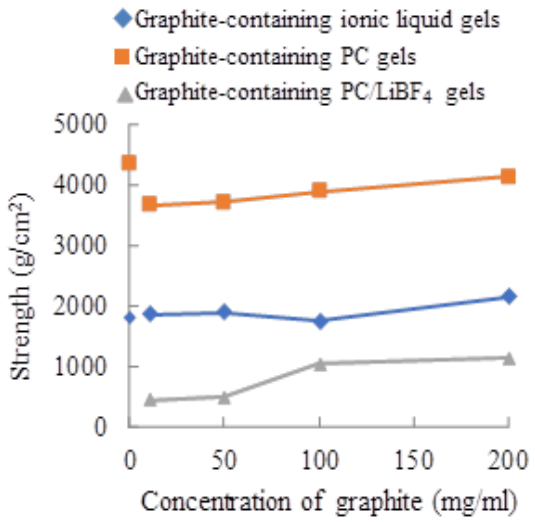

Figure 3.4 Gel strengths of graphite-containing (bmim)BF_4, PC, and $LiBF_4$/PC gels.

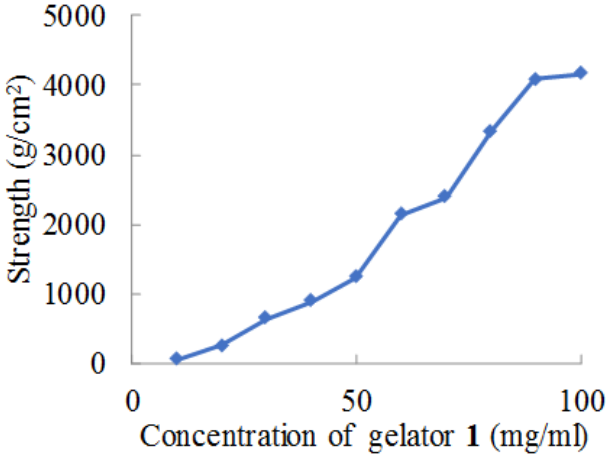

Figure 3.5 Strengths of PC gels prepared from gelator 1

The gels synthesized in this study show a thermally reversible sol-to-gel transition because the 3D networks responsible for gelation are constructed by noncovalent interactions. The gel-to-sol phase-transition temperature increases with increasing concentration of **1**. For instance, the gel-to-sol phase-transition temperatures of PC gels prepared at 20, 50, and 100 mg/mL (**1**/PC) were ~50, 70, and 90°C, respectively (Figure 3.7). We studied the effect of graphite on the phase-transition temperatures of (bmim)BF_4 and PC gels. Figure 3.6 shows the phase-transition temperatures of graphite-containing (bmim)BF_4, PC, and $LiBF_4$/PC gels. The temperatures of the gel-to-sol phase transition for gels prepared at concentrations of 50 mg mL^{-1} (1/(bmim)BF_4) and 100 mg mL^{-1} (**1**/PC) were ~123 and ~90°C, respectively. It is clear from Figure 3.6 that the phase-transition temperature of gels is almost independent of the amount of added graphite; in other words, the hydrogen bonding and van der Waals forces as main driving forces for gelation are not affected by graphite. The temperature of the gel-to-sol transition of graphite-containing $LiBF_4$/PC was observed to be ~50°C, which was low compared with that of graphite-containing PC without $LiBF_4$ (~90°C). The low transition temperature of graphite-containing $LiBF_4$/PC can probably be attributed to the high polarity of PC containing 1 M $LiBF_4$.

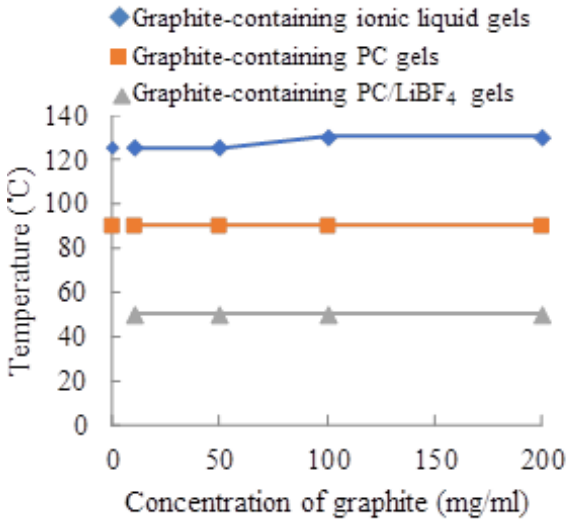

Figure 3.6 Gel-to-sol phase-transition temperatures of graphite-containing (bmim)BF_4, PC, and $LiBF_4$/PC gels.

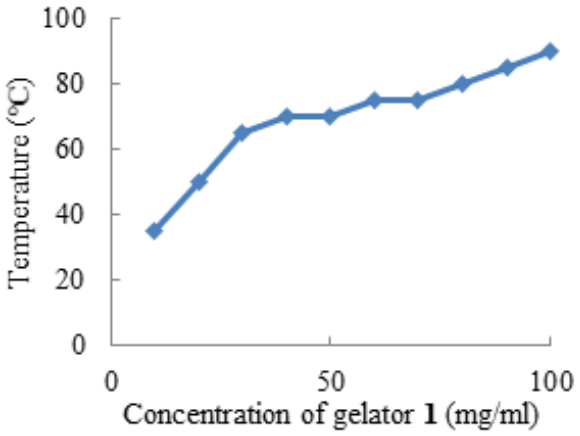

Figure 3.7 Phase-transition temperatures of PC gels prepared from gelator 1

3.3.3 Electrochemical properties

Solid electrolytes, which are electrically conductive solids with ionic carriers, are becoming increasingly important because of their potential use in the fields of solid-state batteries, fuel cells, energy storage, and chemical sensors [22–25]. Gelation of ionic liquids by a gelator is a conventional method for synthesizing gel electrolytes, and recently, the use of thermal scanning conductometry (TSC) was reported in in-situ studies of the conductivity properties, reversibility, and reproducibility of the ionogels based on LMWG [26]. The ionic conductivities of graphite-containing (bmim)BF_4 gels compared with that of pure (bmim)BF_4 are summarized in Table 3.2, for which the concentration of gelator **1** for synthesizing the gels was maintained at 50 mg mL^{-1} and the particle size of graphite was ~45 μm. All the ionic conductivities tests were performed under the condition of 25°C in a temperature-controlled chamber. The ionic conductivities of pure (bmim)BF_4 and (bmim)BF_4 gel formed by **1** (50 mg mL^{-1}) were 4.3 and 4.0 mS cm^{-1}, respectively. Although the ionic conductivity decreased slightly owing to gelation, the ionic conductivity of (bmim)BF_4 gel was high. The result indicates that the gelator molecules hardly interfere with the mobilities of $(bmim)^+$ and BF_4^- as ion carriers. The conductivities of graphite-containing (bmim)BF_4 gels increased on increasing the amount of added graphite; for instance, the conductivities of

(bmim)BF_4 gels containing 100 and 200 mg of graphite were 6.1 and 9.0 mS cm^{-1}, respectively. The definite reason for the increase in ionic conductivity upon adding graphite is unclear; however, we presume that the dissociation of (bmim)BF_4 was accelerated by the π-electrons of graphite. The electronic contribution from graphite in itself will be ignored, because the dispersed graphite particles are isolated in the formed gel and they do not contact with each other.

Table 3.2 Ionic conductivities of pure (bmim)BF_4 and graphite-containing (bmim)BF_4 gels at 25°C.

(bmim)BF_4	gelator **1**	graphite	ionic conductivity	activation energy	state
mL	mg	mg	mS cm^{-1}	kJ mol^{-1}	
1	0	0	4.3	18.6	liquid
1	50	0	4.0	17.8	gel
1	50	10	5.0	16.0	gel
1	50	50	5.3	16.3	gel
1	50	100	6.1	14.6	gel
1	50	200	9.0	10.7	gel

The ionic conductivities of 1 M $LiBF_4$/PC and graphite-containing $LiBF_4$/PC gels are summarized in Table 3.3, for which the concentration of gelator **1** for synthesizing the gels was maintained at 100 mg mL^{-1}. The ionic conductivity of 1 M $LiBF_4$/PC was 4.0 mS cm^{-1}, and the conductivity after gelation by **1** decreased to 3.4 mS cm^{-1}. The slight depression of ionic conductivity upon gelation can be explained by the limited movement of ion carriers in the 3D networks in the gel. The depressed ionic conductivity was recovered by the addition of graphite; for example, the conductivities of 1 M $LiBF_4$/PC gels containing 100 and 200 mg of graphite were 4.4 and 7.1 mS cm^{-1}, respectively. The ionic conductivities of 1 M $LiBF_4$/γ-BL gels denoted the same tendency as that of 1 M $LiBF_4$/PC gels; that is, the conductivities of 1 M $LiBF_4$/γ-BL

gels containing 100 and 200 mg of graphite were 4.5 and 7.7 mS cm^{-1}, respectively.

We also studied the effect of silica gel (particle size 75–150 μm) as a helper additive instead of graphite with the expectation that the silica gel, which comprises polar particles, will accelerate the dissociation of $LiBF_4$ and consequently increase the ionic conductivity. We succeeded in the physical gelation of 1 M $LiBF_4$/PC with the help of silica gel and confirmed the almost similar behavior of the silica-gel-containing gels to the graphite-containing $LiBF_4$/PC gels in terms of gel strength and thermal stability. However, the ionic conductivity was not recovered by adding silica gel; for instance, the conductivities of 1 M $LiBF_4$/PC gels containing 50 and 200 mg of silica gel were 2.3 and 2.2 mS cm^{-1}, respectively. The observation that the silica gel had no effect on increasing the ionic conductivity underlines the importance of the π-electrons of graphite for increasing ionic conductivity. Namely, the π-electrons of graphite would contribute to the additional charge carriers in the gel.

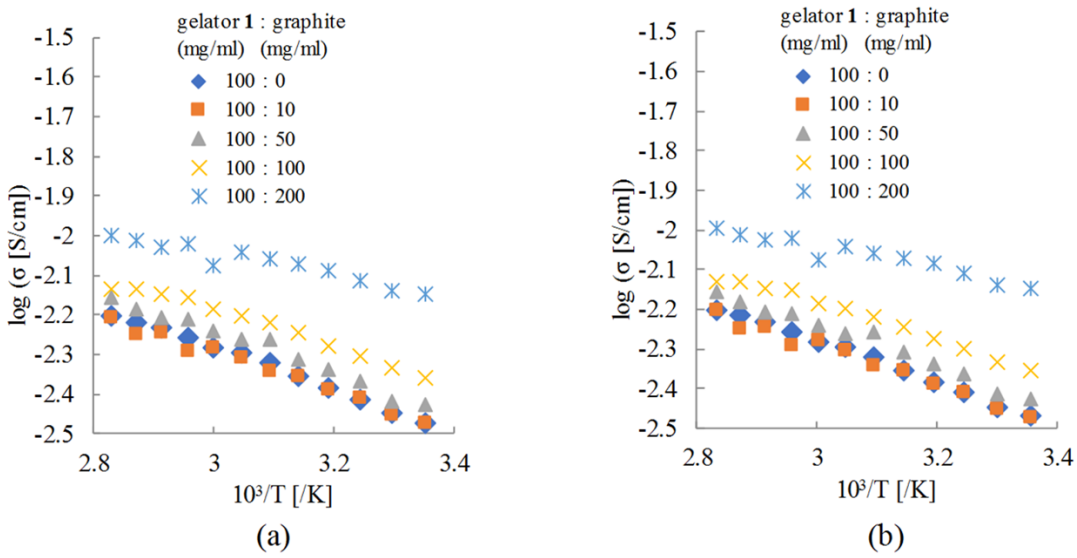

Figure 3.8 Temperature-dependence of ionic conductivities.

(a); graphite-containing (bmim)BF_4 gels

(b); graphite-containing PC/$LiBF_4$ gels

The temperature dependence of ionic conductivity was studied for graphite-containing (bmim)BF_4 and $LiBF_4$/PC gels. Plots of the logarithm of conductivity against 1/T for the graphite-containing (bmim)BF_4 and $LiBF_4$/PC gels were straight lines between 2.83×10^{-3} and 3.25×10^{-3} T^{-1} (Figure 3.8), suggesting that the temperature dependence obeyed the classical Arrhenius plot. The activation energies calculated using the Arrhenius equation are summarized in Table 3.3. The activation energy of the precipitate of 1 M $LiBF_4$/PC containing 100 mg of **1** was 8.1 kJ mol^{-1}, which was greater than that of 1 M $LiBF_4$/PC solution (11.4 kJ mol^{-1}). However, the activation energies of graphite-containing $LiBF_4$/PC gels decreased on increasing the amounts of added graphite. Finally, the activation energy of 1 M $LiBF_4$/PC gel containing 200 mg of graphite decreased to 5.2 kJ mol^{-1}. The decrease in activation energy along with the addition of graphite can be explained by the accelerated dissociation of $LiBF_4$ and the increase of carrier mobility, which are probably caused by the π-electrons of graphite. Notably, the activation energies of silica-gel-containing $LiBF_4$/PC gels were constant, independent of the added silica gel.

Electrochemical stability is a fundamental requirement for applications in electrochemical devices because it determines the highest working potential of the battery. We studied the CV of the 1 M $LiBF_4$/PC solution and 1 M $LiBF_4$/PC gel containing **1** (100 mg mL^{-1}) and graphite (50 mg mL^{-1}) (Figure S3.3). The current increases sharply when the free solvent components in the electrolyte decompose, and the corresponding decomposition voltage represents the upper operating limit. The decomposition voltage of the 1 M $LiBF_4$/PC solution was about 5.5 V, whereas that of graphite-containing 1 M $LiBF_4$/PC gel was much higher than 8 V. The improvement in the decomposition voltage was attributed to the 3D networks of the gel, which affect the ion transfer and stability of the free solvent molecules. Therefore, this clearly demonstrates that the graphite-containing 1 M $LiBF_4$/PC gels may have potential applications for high-voltage lithium ion batteries.

Table 3.3 Ionic conductivities of 1 M $LiBF_4$/PC and graphite-containing $LiBF_4$/PC gels at 25°C.

$LiBF_4$/PC	gelator **1**	graphite	ionic conductivity	activation energy	state
mL	mg	mg	mS cm^{-1}	kJ mol^{-1}	
1	0	0	4.0	8.1	solution
1	100	0	3.4	10.2	precipitate
1	100	10	3.4	9.5	gel
1	100	50	3.7	9.9	gel
1	100	100	4.4	8.7	gel
1	100	200	7.1	5.2	gel

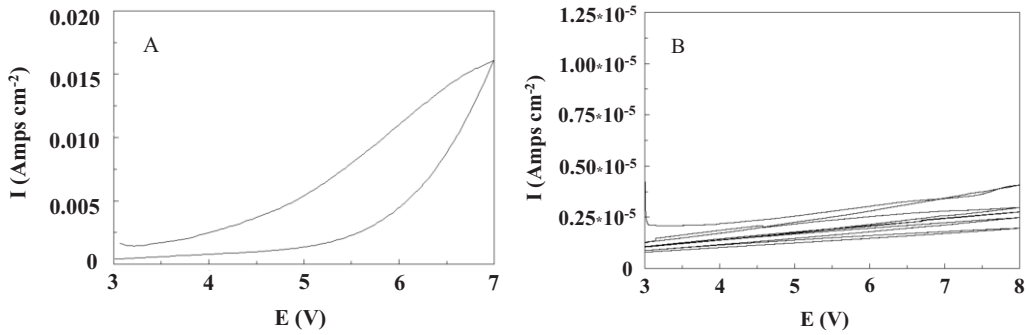

Figure 3.9 CV curves of 1 M $LiBF_4$/PC solution and 1 M $LiBF_4$/PC gel containing **1** (100 mg mL^{-1}) and graphite (50 mg mL^{-1}).

3.4 Conclusion

Gel electrolytes of (bmim)BF_4, PC, and γ-BL were easily obtained by adding gelator **1** to the respective solutions. Gel electrolytes of 1 M $LiBF_4$/PC and 1 M $LiBF_4$/γ-BL were obtained with the help of graphite. Hydrogen bonding among the amide bonds of 1 plays a vital role in the gelation process regardless of the presence of graphite. The effect of graphite on the 3D networks formed by **1** was studied by TEM. Fine, threadlike aggregates with nearly homogeneous diameters were observed in graphite-containing gel electrolytes. The gel strengths of graphite-containing

(bmim)BF_4, PC, and $LiBF_4$/PC gels increased slightly with increasing amounts of added graphite. The gel-to-sol phase-transition temperatures are also almost independent of the amount of added graphite; in other words, the hydrogen-bonding and van der Waals forces as main driving forces for gelation are not affected by graphite. The ionic conductivity of (bmim)BF_4 marginally decreased owing to gelation, indicating that the gelator molecules hardly interfere with the mobility of BF_4^- and BF_4^- as ion carriers. The conductivities of graphite-containing (bmim)BF_4 gels increased with increasing amounts of added graphite. The ionic conductivities of 1 M $LiBF_4$/PC gels slightly decreased owing to gelation, but the depressed ionic conductivity was recovered by the addition of graphite. The increase in the ionic conductivity of the gel electrolytes using graphite as the helper additive was explained by the accelerated dissociation of (bmim)BF_4 and $LiBF_4$ caused by the π-electrons of graphite. Activation energies for ionic conductivity were calculated from the Arrhenius equation. The activation energies of graphite-containing $LiBF_4$/PC gels decreased with increasing amounts of added graphite. Enhanced electrochemical stability was confirmed in graphite-containing 1 M $LiBF_4$/PC gels.

3.5 References

[1] P. J. Flory, Gels and gelling process. *Faraday Discuss. Chem. Soc.,* **1974**, *57*, 7-18.

[2] An, Y., Solids, F. J., Jiang, H. A thermodynamic model of physical gels. *J. Chem. Phys. Solids*, **2010**, *58*, 2083-2099.

[3] P. Terech. R. G. Weiss, Low Molecular Mass Gelators of Organic Liquids and Properties of Their Gels, *Chem. Rev.* **1997**, *97*, 3133-3159.

[4] L. A. Estroff, A. D. Hamilton, Water Gelation by Small Organic Molecular, *Chem. Rev.* **2004**, *104*, 1201-1217.

[5] N. Sangeetha, U. Maitra, Supramolecular gels: Functions and uses, *Chem. Soc. Rev.* **2005**, *34*, 821-836.

[6] M. de Loos, B. L. Feringa, J. H. van Esch, Design and Application of Self-Assembled Low Molecular Weight Hydrogels, *Eur. J. Org. Chem.* **2005**, *17*, 3615-3631.

[7] R. G. Weiss and P. Terech, *Molecular Gels: Materials with Self-assembled Fibrillar Networks*, Springer, Dordrecht, **2006.**

[8] M. Suzuki, K. Hanabusa, L-Lysine-based low-molecular-weight gelators, *Chem. Soc. Rev.* **2009**, *38*, 967-975.

[9] J. Liu, J. Xu, Y. Lin, J. Li, Y. Lai, C. Yuan, J. Zhang, K. Zhu, All-solid-state Lithium Ion Battery: Research and Industrial Prospects. *Acta Chimica Sinica*, **2013**, *71*, 869-878.

[10] W. Li, Z. Li, C. Yang, Q. Xiao, G. Lei, Y. Ding, A capsule-type gelled polymer electrolyte for rechargeable lithium batteries. *RSC Advances*, **2016**, *6*, 47833-47839.

[11] H. Jiang, Y. Zhang, D. Wu, X. Yu, J. Cao, Design and Characterization of High Performance Electrospun Separator for Lithium Ion Battery. *Acta Polym. Sin.*, **2015**, *11*, 1271-1279.

[12] U. Ali, K.J.B.A. Karim, N.A. Buang, A Review of the Properties and Applications of Poly(Methyl Methacrylate)(PMMA). *Polym. Rev.*, **2015**, *55,* 678-705.

[13] Y. Kang, J. Moon, In situ Poly(methyl methacrylate)/Graphene Composite Gel Electrolytes for Highly Stable Dye-Sensitized Solar Cells. *ChemSusChem*, **2015**, *8*, 3799-3804.

[14] H. S. Choe, B. G. Carroll, D. M. Pasquariello, K. M. Abraham, Characterization of Some Polyacrylonitrile-Based Electrolytes. *Chem. Mater.*, **1997**, *9*, 369-379.

[15] W. Kubo, T. Kitamura, K. Hanabusa, Y. Wada, S. Yanagida, Quasi-solid-state dye-sensitized solar cells using room temperature molten salts and a low molecular weight gelator. *Chem. Commun.*, **2002**, *(4)*, 374-375.

[16] S. Sun, J. Song, Z. Shan, R. Feng, Electrochemical properties of a low molecular weight gel electrolyte for supercapacitor. *J. Elcetroanal. Chem.*, **2012**, *676*, 1-5.

[17] V. R. Basrur, J. Guo, C. Wang, S. R. Raghavan, Synergistic Gelation of Silica

Nanoparticles and a Sorbitol-Based Molecular Gelator to Yield Highly-Conductive Free-Standing Gel Electrolytes. *ACS Appl. Mater. Inter.*, **2013**, *5*, 262-267.

[18] L. Li, Q. Zhang, H. Huo, J. Zhou, L. Li, Glutamic acid derivatives as gelators for electrolyte of lithium ion batteries. *RSC Adv*, **2016**, *6*, 88820-88825.

[19] K. Hanabusa, H. Fukui, M. Suzuki, H. Shirai, Specialist Gelator for Ionic Liquids. *Langumuir*, **2005**, *21*, 10383-10390.

[20] K. Hanabusa, K. Hiratsuka, M. Kimura, H. Shirai, Easy Preparation and Useful Character of Organogel Electrolytes Based on Low Molecular Weight Gelator, *Chem. Mater.* **1999**, *11*, 649-655.

[21] K. Hanabusa, M. Matsumoto, M. Kimura, A. Kakehi, H. Shirai, Low molecular weight gelators for organic fluids, Gelation using a family of cyclo(dipeptide)s. *J. Colloid Inter. Sci.*, **2000**, *224*, 231-244.

[22] P. G. Bruce, *Solid State Electrochemistry*, Cambridge University Press: Cambridge, England, **1995**.

[23] M. Z. A. Munshi, *Handbook of Solid State Batteries & Capacitors*; World Scientific: Singapore, **1995**.

[24] P. B. Balbuena, Y. Wang, *Lithium-Ion Batteries: Solid-Electrolyte Interphase*; Imperial College Press: London, England, **2004**.

[25] F. M. Gray, *Solid Polymer Electrolytes: Fundamentals and Technological Applications;* VCH: Germany, **1991**.

[26] M. Bielejewski, K. Nowicka, N. Bielejewska, J. Tritt-Goc, Ionic conductivity and thermal properties of a supramolecular ionogel made from a sugar-based low molecular weight gelator and a quaternary ammonium salt electrolyte solution, *J. Electrochem. Soc.*, **2016**, *163*, 187-195.

Chapter 4

Functional gelators as cathode materials for lithium-ion batteries

4.1 Introduction

A gel is a kind of material that has the properties of both soft and hard matters [1]. Gels are roughly divided into chemical gels and physical ones. Chemical gels, which are usually prepared by polymerization involving multi-functional monomers, are characterized by thermally-irreversibility. The thermally-irreversibility of chemical gels is due to the fact that the three-dimensional networks are built by robust covalent bonds. On the other hand, physical gels always reveal thermally-reversible phase transitions between gel and sol, because their networks are formed through weak non-covalent bonds which are easily broken by heating. For instance, contact lens or intraocular ones are classified in chemical hydrogels; meanwhile, jelly food made with agar is physical hydrogels. Organogels have attracted considerable attention over the past several decades because of their potential applications in energy, biomaterials, bionics, sensors, and drug delivery. The chemical structures of gelators greatly influence the properties of formed organogels because of the different size and shape of three-dimensional networks. Low-molecular-weight gelators (LMWGs) have captured great interest with their interesting properties and potential applications as soft materials in several fields [2-6]. LMWGs form physical gels through non-covalent forces such as hydrogen bonding, van der Waals forces, π–π stacking, electrostatic interactions, etc.

Owing to their competitive energy and power density parameters, lithium-ion batteries (LIBs) have conquered the rechargeable battery market and have numerous potential applications in electronic devices. Since 1970s when LIBs were invented, they have been used worldwide and a lot of research has been dedicated to further improving their performance including energy density, power density, and cycle life [7]. The normal cathode materials for LIBs were generally inorganic solids as $LiCoO_2$ or $LiMnO_4$, which have some special drawbacks like limited theoretical capacity, a non-renewable resource, and huge energy consumption. Organic materials, which could be synthesized with some environmentally benign processes, might adapt to the future

needs of the environment, and also have advantages over inorganic materials such as flexibility and rapidly charge and discharge with a large current [8].

Nitroxide is a kind of stable organic radical that has shown potential in cathode materials [9], polarizing agents [10,11], spin probes [12], magnetoactive materials [13], and radiation protective agents with redox properties of component charge-transfer properties [14,15]. The four α-methyl groups of nitroxide in TEMPO work to make the radical groups stable. For example, Nakahara *et al.* synthesized the stable nitroxyl polyradical poly(2,2,6,6-tetramethyl piperidinyloxy methacrylate) (PTMA) and used it as the cathode active material in rechargeable batteries that exhibited a discharge voltage of 3.5 V and discharge capacity of 77 mA h g^{-1} [16]. Nishide's group synthesized a supramolecular gelator 2,2,6,6-tetramethylpiperidin- -1-oxyl-substituted cyclohexanediamine derivative, demonstrating sol-gel transition around 60 °C and rapid electron self-exchange reaction [17]. Li *et al.* used graphene-grafted PTMA and reduced graphene oxide as cathode materials in a cell that showed a two-electron redox reaction mode, providing a high capacity of 466 mA h g^{-1} [18].

In this paper, we synthesize gelators from 4-NH_2-TEMPO and L-isoleucylamino- -octadecane as a gelation-driving segment. Gelation properties of the gelators are studied in some organic solvents to prove the strong gelation ability. The gel strengths, phase transition temperatures are measured to understand the application conditions of the gel. In addition, cyclic voltammetry and cell behaviours of gel cathode are studied from the standpoint of the potential for use in soft energy storage devices.

4.2 Experimental

4.2.1 Materials

Glutaric anhydride and 4-amino-2,2,6,6-tetramethyl piperidine 1-oxyl (4-NH_2-TEMPO) were purchased from TCI. Succinic anhydride and 1-butyl-3-methyl- -imidazolium tetrafluoroborate ((bmim)BF_4) were purchased from Wako.

L-Isoleucylaminooctadecane was prepared by the deprotection reaction of the carbobenzyloxy group of *N*-carbobenzyloxy-L- -isoleucyaminnooctadocane [19]. All of the solvents were used without further purification.

4.2.2 Sample preparation

FT-IR spectra were measured with a JASCO FS420 spectrometer with the KBr method. Compound **2a** and **2b** were synthesized by an addition reaction with L-isoleucylaminooctadecane and succinic anhydride or glutaric anhydride as reported by our previous work [20].

Compound **3a** and **3b** were synthesized by an amidation reaction between 4-NH_2-TEMPO and compound **2a/2b**. A mixture of 4-NH_2-TEMPO (2.75 g, 16 mmol), **2a** (7.7 g, 16 mmol), *N,N'*-diisopropyl- -carbodiimide (DIC; 2.21 g, 17.6 mmol)), and 4-dimethylaminopyridine (DMAP; 1.9 g, 16 mmol) in dry CH_2Cl_2 (50 mL) were refluxed overnight. After the evaporated, the crude product was first recrystallized in THF (30 mL) and then in methanol (20 mL). Finally, recrystallization from dichloromethane/ether (20/400 mL) gave an orange product.

3a: Yield: 70%; FT-IR (cm^{-1}): 3286 (υ N-H amide), 1634 (υ C=O, amide I), 1544 (δ N–H, amide II); Elemental analysis (%) calculated: C 69.88, H 11.25, N 8.81; Found: C 69.65, H 11.66, N 8.85.

3b: Yield: 55%; FT-IR (cm^{-1}): 3286 (υ N-H amide), 1634 (υ C=O, amide I), 1544 (δ N–H, amide II); Elemental analysis (%) calculated: C 70.22, H 11.32, N 8.62; Found: C 69.39, H 11.59, N 9.05.

4.2.3 Gelation tests

Gelation tests were performed by using test tubes (the inside diameter; 14 mm) with gelators and organic solvents inside. Each sample was dissolved in a solvent by heating and then cooled to 25 °C for 2 h. Gel formation was determined visually by inverting the test tube.

4.2.4 TEM observation

Transmission electron microscopy (TEM) was conducted on a JEOL-2010 electron microscope with the voltage of 200 kV. Each sample was prepared below the minimum gelation concentration, and then dropped onto a grid coated with a carbon film. After drying in a vacuum for 3 days, each sample was negatively stained with osmium tetroxide overnight.

4.2.5 Electrochemistry

Cyclic voltammograms (CV) were measured with a Solartron SI 1287 electrochemical interface (TOYO Corporation). One 0.27-cm-thick Teflon plant with a 0.3 cm radius hole was adhered to the electrochemical interface setup with insulation tape on both sides. The gelator was dissolved in 1 mL of propylene carbonate (PC) or γ-butyrolactone (γ-BL) containing 1 M $LiBF_4$. After heating, the sample was added through the hole into a Teflon mold. The Teflon mold was then sandwiched between two pieces of ITO electrodes and placed in an oven at 25 °C for 2 h to make it stable.

The cathode for the test half-cell was made by mixing the gelator (70 μg), acetylene black (20 μg), and PVDF (10 μg) in 1-methyl-2-pyrrolidone (NMP) (100 μL). After heating, the mixture was sonicated overnight to make sure it homogeneous. The mixture was spin-coated on aluminum foil (1 cm^2) and dried overnight at 40 °C to form a xerogel cathode. The prepared cathode was directly assembled in a glove-box under a dry helium gas atmosphere into a CR2025 coin-type half-cell with lithium foil as the anode, where a PP film (Celgard 2500) was used as a separator. An 1 M $LiPF_6$ solution in ethylene carbonate (EC), diethyl carbonate (DEC) and $(BMIM)BF_4$ (vol.-ratio; 3:3:4) was used as the electrolyte [21].

4.3 Results and discussion

4.3.1 Gelation ability

We have proposed a concept of the gelation-driving segment for the purpose of developing various types of gelator [22]. We reported the extraordinarily strong gelation

ability of N-benzyloxycarbonyl-L-isoleucylaminooctadecane [19] and supposed that L-isoleucylaminooctadecane is one of the gelation-driving segments. In fact, several compounds derived from L-isoleucylaminooctadecane exhibit gelation ability [22]. In the present study, we focused on L-isoleucylaminooctadecane as a gelation-driving segment and prepared **2a**. Figure 4.1 shows the synthesis steps of the gelators which containing the redox-active organic compounds and amino acid derivatives. Amino acid derivatives with strong gelation abilities had been reported as LMWGs [23]. In normal LIBs, the cathode material is usually in the solid state, which means that neither the size nor the shape can be changed after manufacture. However, gel cathodes and electrolytes could lead to batteries with changeable size and shape for different applications. We synthesized gelators (**3a** and **3b**) and studied the gelation behaviour in PC and γ-BL,

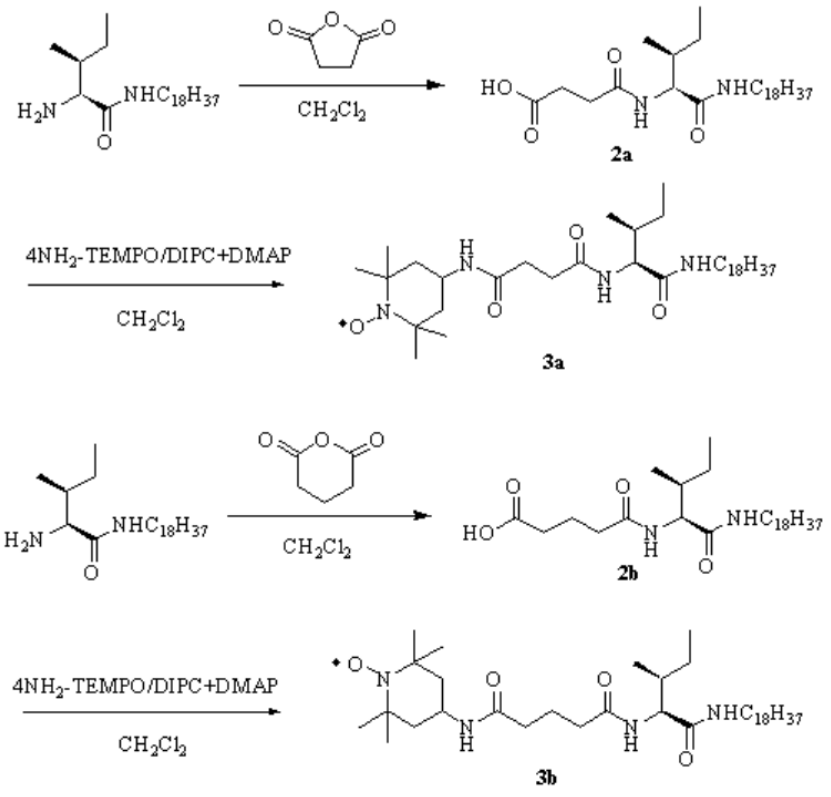

Figure 4.1 Synthesis of **3a** and **3b**

which were used as the electrolyte solvent in LIBs, and other normal organic solvents. The results of the gelation tests are summarized in Table 4.1. Both of **3a** and **3b** showed excellent performances in organic solvents, especially in PC and γ-BL. The minimum gelation concentration was 4 mg mL^{-1}, which showed the better performance in tested liquids. For gel-type cathodes, the presence of lithium salt is needed to facilitate ion transport. Therefore, we added different lithium salts to the gels as electronic conductors. The results are shown in Table 4.2. The minimum gelation concentration increased with the concentration of lithium salt. The change of minimum gelation concentration can be ascribed to the dielectric constant of γ-BL increased by addition of lithium salt.

Table 4.1 Gelation properties of **3a** and **3b** in organic solvents at 25 ℃

solvent	**3a**	**3b**
Hexane	GTL(20)	GTL(20)
Methanol	GTL(40)	GTL(40)
Acetone	GT (10)	GO(40)
IPM	GTL(10)	GO(20)
THF	S	PG
DMF	GT(40)	GT (20)
DMSO	GT(8)	GT (20)
PC	GTL(4)	GTL(4)
γ-BL	GT(4)	GT (4)
Toluene	GT(8)	GT (40)
Nitrobenzene	GT10)	GT(4)
Acetonitrile	GTL(8)	GO(10)

Values mean minimum gelation concentrations (mg mL^{-1}) GT: Transparent gel, GTL: Translucent gel, GO: Opaque gel, PG: Partial gel at 40 mg mL^{-1}, S: Solution at 40 mg mL^{-1}.

Table 4.2 Gelation properties of **3a** and **3b** in γ-BL with lithium salts at 25 ℃

solvent	**3a**	**3b**
$LiBF_4$(1 M)	GTL(20)	GTL(20)
$LiBF_4$(0.1 M)	GTL(10)	GTL(10)
$LiBF_4$(0.01 M)	GTL(8)	GTL(8)
$LiClO_4$(1 M)	GTL(20)	GTL(20)
$LiClO_4$(0.1 M)	GTL(10)	GTL(10)
$LiClO_4$(0.01 M)	GTL(8)	GTL(8)

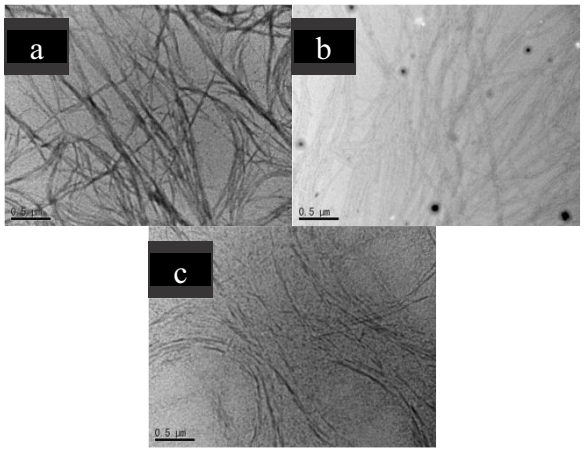

Figure 4.2 TEM images of gelator **3a**:

(a) Xerogel prepared from γ-BL at 0.8 mg mL^{-1}.

(b) Xerogel prepared from 1M $LiBF_4$/γ-BL at 2.0 mg mL^{-1}.

(c) Xerogel prepared from 1M $LiClO_4$/γ-BL at 2.0 mg mL^{-1}.

4.3.2 Morphology

The influence of the lithium salt on the three-dimensional networks formed by the gelator was studied by TEM. Figure 4.2 shows TEM images of gels with γ-BL, $LiBF_4$/γ-BL, and $LiClO_4$/γ-BL, which were prepared by cooling the corresponding warmed solutions. The image of xerogel prepared from loose gel in γ-BL at 0.8 mg mL^{-1} showed clear fibers with a diameter of ~100 nm, while the fibers of γ-BL with $LiBF_4$ or

$LiClO_4$ showed diameters of ~40 nm. The slender fibers in γ-BL with Li salts suggest that the lithium salt obstructed the aggregation of the gelator, making it difficult to form a gel.

4.3.3 Gel strength and thermal stability

Gel strength is an important factor in the application of gels. It has been evaluated by elastic storage modulus *G'* and loss modulus *G''* values. Here we evaluated gel strength as the power necessary to sink a cylindrical bar (10 mm in diameter) 4 mm deep into each gel.[23,24] Gel strength usually increases nearly in proportion to the amount of gelator added [19,23]. The gel strengths of γ-BL gels are shown in Figure 4.3. The gel strength of γ-BL gel with a concentration of 20 mg mL^{-1} of **3a** was over 800 g cm^{-2}. The gel strength of the gels containing lithium salt was decreased to 50 g cm^{-2} for the same concentration of **3a**. This result also indicates that the lithium salt obstructed the growth of fibrous aggregation. Since the gel strengths depended on the concentration of the gelators, the gels with demanded gel strengths can be prepared. Soft batteries with different strength demands can be prepared by using gelators.

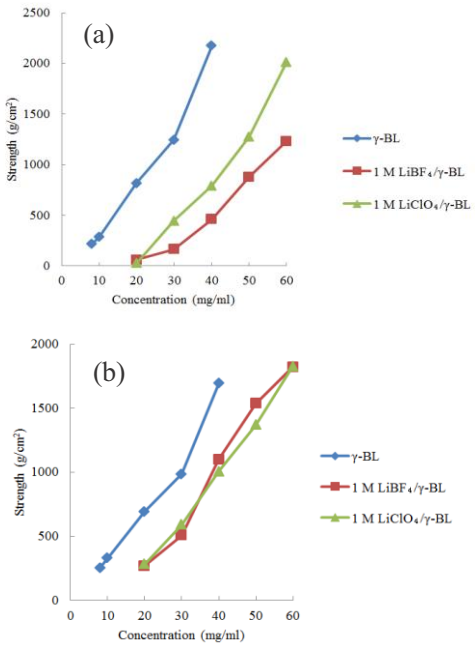

Figure 4.3 Gel strengths of the gels of prepared with **3a** (a) and **3b** (b).

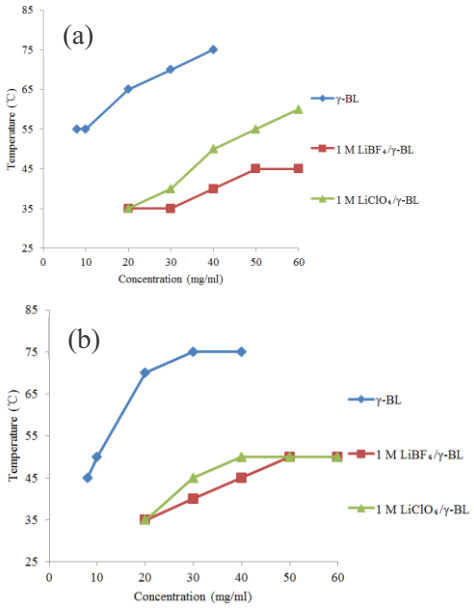

Figure 4.4 Gel-sol transition temperatures of the gels of prepared with **3a** (a) and **3b** (b).

The gels showed thermally reversible sol–gel transitions, which were attributed to the three-dimensional gel networks constructed by non-covalent interactions. The phase transition temperatures between the gel and sol increased with the concentrations of both **3a** and **3b** (Figure 4.4). The sol–gel transition temperatures could decide the operation temperature for a battery, and might have the ability to protect the battery from explosion at high temperature through the phase change between the gel and sol.

4.3.4 Electrolyte properties

The properties of cathode materials currently limit the development of energy storage devices [25]. To better understand the gel-type cathodes, the electrolyte properties of the gels were studied, demonstrating the electroactivity and reversible redox behaviour of the gelators. Figure 4.5 and Figure 4.6 show CV measurements of gel-electrolytes which were performed using a sandwich coin-type setup with ITO electrodes, and the concentration of gelator was 20 mg mL^{-1} in 1 M $LiBF_4$/γ-BL solution. Nearly the same results were observed for the sample **3a** and **3b**. Both cathode

and anode peaks were observed at 0.4 V for **3a**. The almost same redox properties were observed for the gel made of the raw material 4-NH_2 TEMPO and gelator **2a**.This shows that the electrochemical activities of the radical in the gel made of **2a** and that of the gel of **3a** were approximately identical.

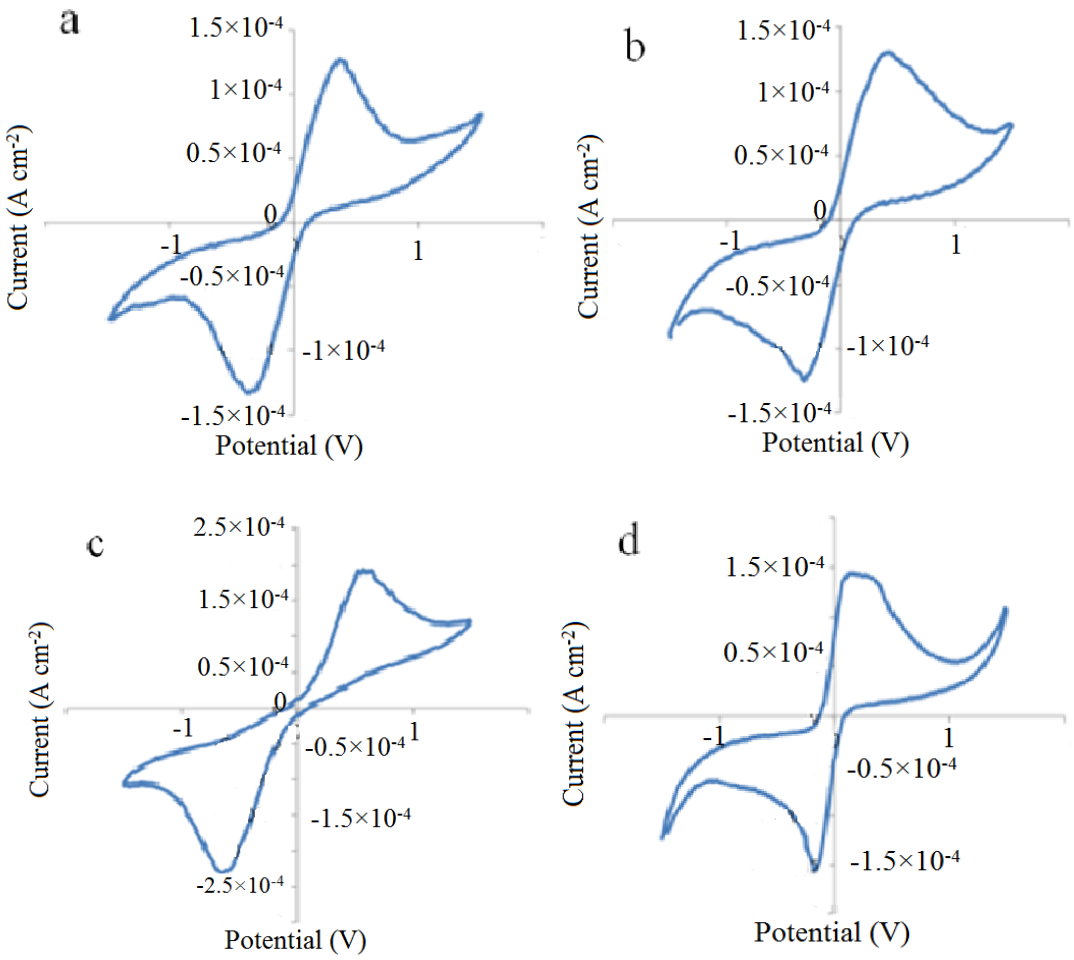

Figure 4.5 Cyclic voltammograms of gel-electrolytes after 5 cycles. The scan rate was 200 mV s^{-1}.

(a) 20 mg mL^{-1} of **3a** in 1M $LiBF_4$/γ-BL.

(b) 20 mg mL^{-1} of **3b** in 1M $LiBF_4$/γ-BL.

(c) 15 mg mL^{-1} of **2a** and 5.45 mg mL^{-1} of 4NH_2-TEMPO in 1M $LiBF_4$/γ-BL.

(d) 15 mg mL^{-1} of **2b** and 5.45 mg mL^{-1} of 4NH_2-TEMPO in 1M $LiBF_4$/γ-BL.

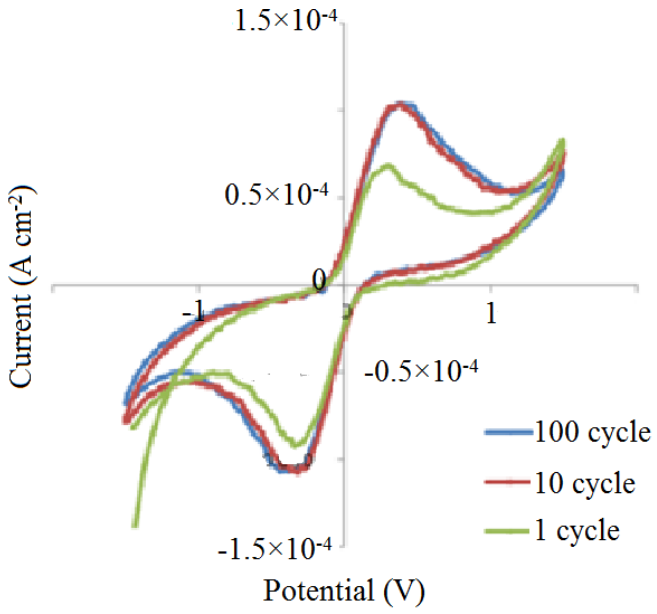

Figure 4.6 Cyclic voltammograms of gel-electrolyte prepared from 20 mg mL^{-1} of **3a** in γ-BL. Scan rate was 200 mV s^{-1}.

In the CV experiments, the oxidation peak in the first cycle was smaller than that in the others due to the formation of a solid-electrolyte interface film and its thermal oxidation during preparation and handling. The samples showed a linear correlation between I_p and the concentration of **3a** (Figure 4.7). The linear plots were performed to determine the diffusion coefficient (D) of the electro active species. The peak current increased with increasing the concentration of **3a**, confirming that the amount of redox also increased. With the increasing of the gelator concentration, the oxidation peak voltage also increased, which is probably caused by polarization and the ohmic potential drop (*IR* drop) [26].

Because of equipment limitations, a half-cell was fabricated with normal solid cathode materials. The cathode composite material was prepared by ball-milling a mixture of 70% gelator, 20% acetylene black, and 10% PVDF binder in NMP. Charge and discharge cycling was conducted at 1 C (0.037 mA). The half-cells were first discharged to 2 V and then charged to 4.0 V. During the charging process, the radical functional group in the cathode was oxidized to the oxoammonium cation. During the

discharging process, the nitroxide radical was regenerated by the reduction of the oxoammonium cation (Figure 4.8). A nearly constant voltage plateau between 3.65 and 3.55 V was observed, which was almost the same that reported previously for PTMA [26]. The discharge capacity of the first cycle was 40 mA h g^{-1}, while the theoretical capacity was 42 mA h g^{-1}. In the second cycle, the capacity decreased to 21 mA h g^{-1}, because of the partial dissolve of the gelator, and that of the third cycle was about 18 mA h g^{-1}. After ten cycles, the capacity decreased to 10 mA h g^{-1} and the corresponding Coulomb efficiency was over 96% (Figure 4.9 and Figure 4.10). Although this half-cell performance is not good enough, the CV performance of the gels confirmed the stability of the present gelators. We confirmed the possibility of realizing gel-type cathodes with gel-type electrolytes by these tests. These materials may have potential applications in some soft equipment like electronic storage devices for clothes and IC cards.

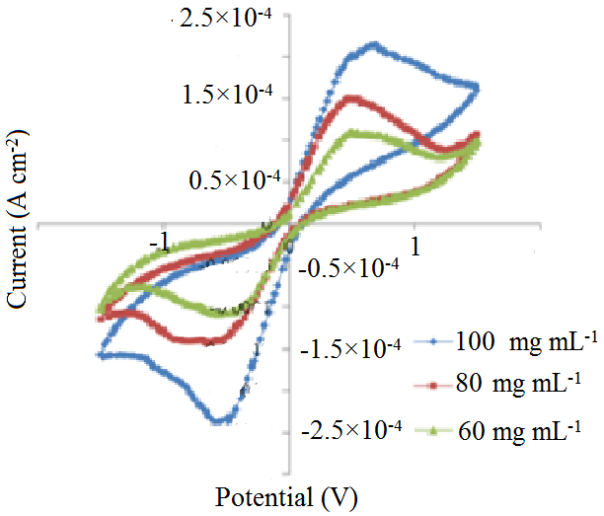

Figure 4.7 Cyclic voltammograms of gel-electrolytes of 1 M $LiBF_4$/γ-BL containing different concentration of **3a**.

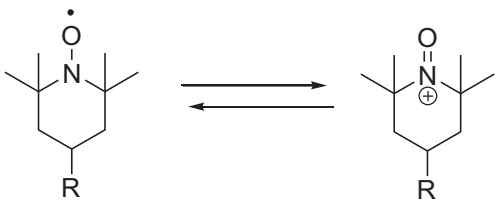

Figure 4.8 Redox of TEMPO (left) and $TEMPO^+$ (right)

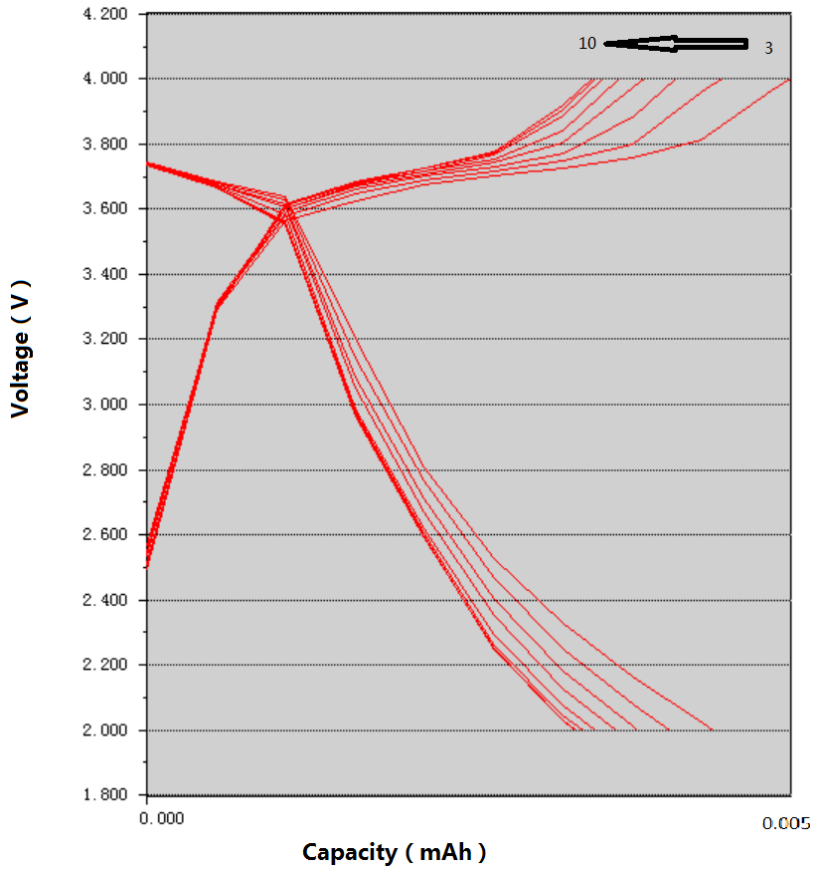

Figure 4.9 Charge and discharge curves of half-cell with gelator-containing cathode from cycle 3 to 10. The charge/discharge rate was set at 1 C.

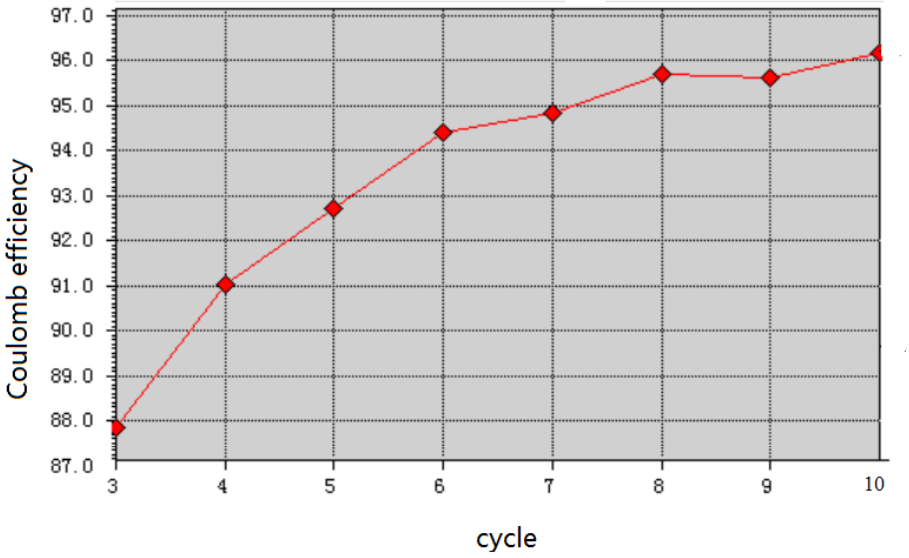

Figure 4.10 Coulomb efficiency curve of the half-cell with gelator containing cathode from cycle 3 to 10. The charge/discharge rate was set at 1 C.

4.4 Conclusions

We synthesized TEMPO-containing gelators that easily form gels with various organic solvents. The three-dimensional network structure of the gels was studied by TEM observation. Compared with the gel without lithium salt, the lithium salt containing gel shows that lithium salt obstructed the growth of the fibrous aggregation and leads to the decreasing of the gel strength. Furthermore, the different concentrations of the gelator could make it possible to fit for different strength demands. The gel-sol transition temperatures delimit the operation temperatures of the gels and could be useful to control the working temperature in some potential applications. CV tests revealed the stability and redox property of the gel-form cathode. Although the gel cathodes did not exhibit good performance in normal half-cell tests, the electrical stability of the gels were confirmed. The TEMPO-containing gelators have the potential to become an excellent class of rapid charge-transporting and energy storage soft materials with widely applications.

4.5 Acknowledgements

We thank Prof. Chenglin Yan of Soochow University for assistance with the experiments and also thank Dr. Tao Qian of Soochow University for valuable discussions.

4.6 References

[1] J. D. Ferry, Viscoelastic Properties of Polymers, 3rd Edition, Wiley-VCH, New York, **1980**.

[2] P. Terech, R. G. Weiss, Low-Molecular Mass Gelators of Organic Liquids and the Properties of their Gels, *Chem. Rev.*, **1997**, *97*, 3133-3159.

[3] L. A. Estroff, A. D. Hamilton, Water Gelation by Small Organic Molecules, *Chem. Rev.* **2004**, *104*, 1201-1217.

[4] N. Sangeetha, U. Maitra, Supramolecular gels: Functions and uses, *Chem. Soc. Rev.* **2005**, *34*, 821-836.

[5] M. de Loos, B. L. Feringa, J. H. van Esch, Design and Application of Self-Assembled Low Molecular Weight Hydrogels, *Eur. J. Org. Chem.* **2005**, *17*, 3615-3631.

[6] R. G. Weiss and P. Terech, *Molecular Gels: Materials with Self-assembled Fibrillar Networks*, Springer, Dordrecht, **2006.**

[7] J. B. Goodenough, K.-S. Park, The Li-ion Rechargeable Battery: A perspective, *J. Am. Chem. Soc.,* **2013**, *135*, 1167-1176.

[8] H. Nishide, K. Oyaizu, Toward Flexible Batteries, *Science*, 2008, *319*, 737-738.

[9] K. Oyaizu, H. Nishide, Radical polymers for Organic Electronic Devices: A Radical Departure from Conjugated polymers?, *Adv. Mater*. **2009**, *21*, 2339-2344.

[10] C. Ysacco, E. Rizzato, M. A. Virolleaud, H. Karoui, A. Rockenbauer, F. Le Moigne, D. Siri, O. Ouari, R. G. Griffin, P. Tordo, Properties of dinitroxides for use in dynamic nuclear polarization (DNP), *Phys. Chem. Chem. Phys.* **2010**, *12*, 5841-5845.

[11] E. L. Dane, B. Corzilius, E. Rizzato, P. Stocker, T. Maly, A. A. Smith, R. G. Griffin, O. Ouari, P. Tordo, T. M. Swager, Ragid Orthogonal Bis-TEMPO Biradicals with Improved Solubility for Dynamic Nuclear Polarization, *J. Org. Chem.* **2012**, *77*, 1789-1797.

[12] Z. Zhelev, R. Bakalova, I. Aoki, K. Matsumoto, V. Gadjeva, K. Anzai, I. Kanno Nitroxyl radicals as low toxic spin-labels for non-invasive magnetic imaging of blood-brain barrier permeability for conventional therapeutics, *Chem. Commun.* **2009**, *(1)*, 53-55.

[13] Y. Wu, Y. Hirai, Y. Tsunobuchi, H. Tokoro, H. Eimura, M. Yoshio, S. Ohkoshi, T. Kato, Supramolecular approach to the formation of magneto-active physical gels,

Chem. Sci. **2012**, *3*, 3007-3010.

[14] A. P. Cotrim, F. Hyodo, K. Matsumoto, A. L. Sowers, J. A. Cook, B. J. Baum, M. C. Krishna, J. B. Mitchell, Differential Radiation Protection of Salivary Glands versus Tumor by Tempol with Accompanying Tissue Assessment of Tempol by Magnetic Resonance Imaging, *Clin. Cancer. Res.* **2007**, *13*, 4928-4933.

[15] S. Nakatsuji, K. Aoki, A. Kojoh, H. Akutsu, J. Yamada, M. Karakawa, Y. Aso, Self-Assembling Aryl-Naphthalendiimide Derivatives with a Nitroxide Radical, *Asian J. Org. Chem.* **2013**, *2*, 164-168.

[16] K. Nakahara, S. Iwasa, M. Satoh, Y. Morioka, J. Iriyama, M. Suguro, E. Hasegawa, Rechargeable batteries with organic radical cathodes, *Chem. Phys. Lett.* **2002**, *359*, 351-354.

[17] Y. Sasada, R. Ichinoi. K, Oyaizu, H. Nishide, Supramolecular Organic Radical Gels Formed with 2,2,6,6-Tetramethylpiperidin-1-oxyl-substituted Cyclohexanediamines: A Very Efficient Charge-Transporting and –Storable Soft Material, *Chem. Mater*., **2017**, *29*, 5942-5947.

[18] Y. Li, Z. Jian, M. Lang, C. Zhang, X. Huang, Covalently Functionalized Graphene by Radical Polymers for Graphene-Based High-Performance Cathode Materials, *ACS Appl. Mater. Inter.*, **2016**, *8*, 17352-17359.

[19] K. Hanabusa, K. Hiratsuka, M. Kimura, H. Shirai, Easy Preparation and Useful Character of Organogel Electrolytes Based on Low Molecular Weight Gelator, *Chem. Mater.* **1999**, *11*, 649-655.

[20] Z. Wang, S. Fujisawa, M. Suzuki, K. Hanabusa, Low Molecular Weight Gelators Bearing Elcetroactive Groups as Cathode Materials for Rechargeable Batteries, *Macromol. Symp.*, **2016**, *364*, 38-46.

[21] M. Diaw, A.Chagnes, B. Carre, P. Willmann, D. Lemordant, Mixed ionic liquid as electrolyte for lithium batteries, *J. Power Sources*, **2005**, *146*, 682-684.

[22] K. Hanabusa, M. Suzuki, Physical gelation by low-molecular-weight compounds and development of gelators, *Bull. Chem. Soc. Jpn*, **2016**, *89*, 174-182.

[23] K. Hanabusa, H. Fukui, M. Suzuki, H. Shirai, Specialist Gelator for Ionic Liquids, *Langmuir*, **2005**, *21(23)*, 10383-10390.

[24] H. Nakagawa, M. Suzuki, K. Hanabusa, Physical gelation by amides derived from trans-1,2-diaminocyclohexane and their tetrasiloxane-based gelators, *Polym. J.*, **2017**, *49(5)*, 439-447.

[25] M. Lin, M. Gong, B. Lu, Y. Wu, D. Wang, M. Guan, M. Angell, C. Chen, J. Yang, B. Hwang, H. Dai, An ultrafast rechargeable aluminum-ion battery, *Nature*, **2015**, *520*, 324-328.

[26] B. Yan, C. Lim, Z. Song, L. Zhu, Analysis of Polarization in Realistic Li Ion Battery Electrode Microstructure Using Numerical Simulation, *Electrochim. acta*, **2015**, *185*, 125-141.

[27] M. Aydin, B. Esat, Ç. Kilic, M. E. Koese, A. Ata, F. Yilmaz, A polythiophene derivative bearing TEMPO as a cathode material for rechargeable batteries, *Eur. Polym. J.*, **2011**, *47*, 2283-2294.

Chapter 5

Conclusion and prospects

5.1 Conclusion

With the growing requirements of renewable energy and green chemistry, the demand for LIBs is continuously increasing. This paper describes the history of the gels and LIBs, and I have performed some research on gel-type electrolytes and gel-type cathodes. The results are shown in follows.

Chapter 2, describes the synthesis of two compounds that have a nitroxide radical and a gelation driving segment, and their gelation ability in organic solvents was investigated. AFM and TEM showed that our samples constituted a 3D network of fibrous aggregates that immobilized the solvent molecules. The redox properties of our compounds were investigated, and it was shown that the electroactivity of the xerogel was much higher than that of the raw material. However, with the increasing of the concentration and the network structure might obstruct the movement of Li^+ ions and hinders its redox properties.

Chapter 3, describes how gel electrolytes of (bmim)BF_4, PC, and γ-BL were easily obtained by adding gelator to the respective solutions. Gel electrolytes of 1 M $LiBF_4$/PC and 1 M $LiBF_4$/γ-BL were obtained with the help of graphite. Hydrogen bonding among the amide bonds of 1 plays a vital role in the gelation process regardless of the presence of graphite. Fine, threadlike aggregates with nearly homogeneous diameters were observed in graphite-containing gel electrolytes. The gel strengths of graphite-containing (bmim)BF_4, PC, and $LiBF_4$/PC gels increased slightly with the amount of added graphite. The gel-sol phase-transition temperatures are also almost independent of the amount of added graphite; in other words, the hydrogen-bonding and van der Waals forces, as the main driving forces for gelation are not affected by graphite. The ionic conductivity of (bmim)BF_4 marginally decreased owing to gelation, indicating that the gelator molecules hardly interfere with the mobility of BF_4^- and BF_4^- as ion carriers. The conductivities of graphite-containing (bmim)BF_4 gels increased with the amount of added graphite. The ionic conductivities of 1 M $LiBF_4$/PC gels slightly

decreased owing to gelation, but the depressed ionic conductivity was recovered by the addition of graphite. The increase in the ionic conductivity of the gel electrolytes with graphite as an additive was explained by the accelerated dissociation of (bmim)BF_4 and $LiBF_4$ caused by the π-electrons of graphite. The activation energies of graphite-containing $LiBF_4$/PC gels decreased as the amount of added graphite. Enhanced electrochemical stability was confirmed in graphite-containing 1 M $LiBF_4$/PC gels.

Chapter 4 describes the synthesis of TEMPO-containing gelators that easily form gels with various organic solvents. The three-dimensional network structure of the gels was studied by TEM observation. Compared with the gel without lithium salt, the lithium salt containing gel shows that lithium salt obstructed the growth of the fibrous aggregation and leads to the decreasing of the gel strength. Furthermore, the different concentrations of the gelator could make it possible to fit for different strength demands. The gel-sol transition temperatures delimit the operation temperatures of the gels and could be useful for controlling the working temperature in some potential applications. CV tests revealed the stability and redox properties of the gel-form cathode. Although the gel cathodes did not exhibit good performances in normal half-cell tests, the electrical stability of the gels was confirmed.

In summary, I synthesized a series of low-molecular-weight gelators which has the potential applications as cathode materials and LMWG electrolytes. The TEMPO-substituted gelators formed three-dimensional network structures in the suitable solvents and showed rapidly redox properties with both gel and xerogels. The cyclo(L-β-3,7-dimethyloctylasparaginyl-L-phenylalanyl) showed the excellent gelation properties with a commercial electrolyte and showed a slight decrease in conductivity compared with a liquid electrolyte due to its three-dimensional structure.

5.2 Prospects

This paper describes research on novel cathode materials and electrolytes for the LIBs. Further research is required:

(1) The capacity of our compounds is insufficient for the applications in daily life due to the size of functional compounds in gelator. It is possible to increase the amount of radical in the side chains.

(2) Due to the demand for soft batteries, further research on soft gels is needed, as soft anodes.

Chapter 6
Acknowledge

Acknowledge

It is my pleasure to write this message and express my gratitude to all those who have directly or indirectly contributed to the creation of this thesis.

First of all, I would like to express my deepest gratitude to Prof. Kenji Hanabusa, my supervisor, and Prof. Masahiro Suzuki for their continuous instruction with important suggestion, precious advice as well as their enduring patience, fruitful encouragement and large support thorough my doctoral course in Shinshu University.

I would like to express my gratitude to the reviewers, Prof. Kenji Hanabusa, Prof. Masahiro Suzuki, Prof. Limin Bao, Prof. Musubu Ichikawa and Prof. Hiromori Tsutsumi for their kind supports and their invaluable comments and insights. Their advice, insightful comments and suggestions provided significant support on this work.

Naturally, these studies have joint efforts with many other researchers. Thanks also would be given to my group-mates, senior members and juniors for their joining part of experiment work, as well for pleasant and enjoyable work environment that they made.

I sincerely appreciate the Grant-in-Aid for the International Fiber Engineering Course of Shinshu University and Chinomori Scholarship from Shinshu University and the Rotary Yoneyama Memorial Foundation for their financial support.

I also acknowledge with pleasure to Prof. Chenglin Yan of Soochow University for assistance with the experiments and also thank Dr. Tao Qian of Soochow University for valuable discussions.

I would like to say that I am very lucky to meet lots of kind friends during learning career in Ueda. They are always there, to laugh with me in the happy times and to lend a helping hand, when I meet difficulties. We share many experiences and help each other. I am heartily grateful to all my friends at Shinshu University for playing along with me and making the wonderful clips and precious memories of my twenties lives.

I dedicate my greatest thanks to my beloved family. Words fail to express my deep gratitude to my parents for their patience, understanding, love, meticulous care and

unlimited support over the years.

Chapter 7

List of publications

List of publications

[1] Z. Wang, S. Fujisawa, M. Suzuki, K. Hanabusa, Low Molecular Weight Gelators Bearing Electroactive Groups as Cathode Materials for Rechargeable batteries, *Macromol. Symp.*, **2016**, *364,* 38-46

[2] Z. Wang, S. Fujisawa, M. Suzuki, K. Hanabusa, Easy preparation of graphite-containing gel electrolytes using a gelator and characterization of their electrochemical properties, *Soft Mater.*, **2017**, *3*, 214-221.

[3] Z. Wang, S. Fujisawa, M. Suzuki, K. Hanabusa, Functional gelators as cathode materials for lithium-ion batteries, *J. Fiber Sci. Technol.,* **2018***,74*,47-53.